NUMERICAL SIMULATION OF SQUEEZE FILM DAMPERS AND

STUDY OF THE EFFECT OF CENTRAL GROOVE ON THE

DYNAMIC PRESSURE DISTRIBUTION

A Thesis

by

PRANEETHA BOPPA

Submitted to the Office of Graduate Studies of
Texas A&M University
in partial fulfillment of the requirements for the degree of

MASTER OF SCIENCE

August 2011

Major Subject: Mechanical Engineering

NUMERICAL SIMULATION OF SQUEEZE FILM DAMPERS AND

STUDY OF THE EFFECT OF CENTRAL GROOVE ON THE

DYNAMIC PRESSURE DISTRIBUTION

A Thesis

by

PRANEETHA BOPPA

Submitted to the Office of Graduate Studies of
Texas A&M University
in partial fulfillment of the requirements for the degree of

MASTER OF SCIENCE

Approved by:

Chair of Committee,   Gerald L. Morrison
Committee Members,   Andrew Duggleby
                      Gioia Falcone
Head of Department,   Dennis O'Neal

August 2011

Major Subject: Mechanical Engineering

ABSTRACT

Numerical Simulation of Squeeze Film Dampers and Study of the Effect of Central

Groove on the Dynamic Pressure Distribution. (August 2011)

Praneetha Boppa, B-tech, National Institute of Technology Warangal, India

Chair of Advisory Committee: Dr. Gerald Morrison

Squeeze film dampers are used in the high speed turbo machinery industry and aerospace industries as a means to reduce vibration amplitude, to provide damping, to improve dynamic stability of the rotor bearing system and to isolate structural components. The effects of cavitation included in previous studies were not effective. The effect of different design parameters were not studied thoroughly as experimental investigation of squeeze film dampers is very expensive. Few of them used numerical investigation but the methods they used are either time consuming or complicated. The present study investigated the feasibility of applying a steady state solver, which is computationally less expensive, for analyzing flow field inside the squeeze film dampers. The behavior of dynamic pressure profiles at different operating conditions, and the effect of a central groove on dynamic pressure profiles were also studied. Simulation results of a 3D case which is similar to the one experimentally studied by Delgado, A., 2008 were used to establish if the moving reference frame (MRF) model in Fluent 12.1 can be used. A steady state solver in an absolute frame of reference was used to produce whirling motion of the rotor in this study. The inlet pressure of 31kpa and the

whirling speed of 50 and 100Hz were used as boundary conditions. The mixture model with three percent dissolved air in lubricant is used to model multiphase flow. Singhal cavitation model is used to model cavitation. The simulations (50,000 iterations) were run until steady state solutions were reached. The results closely agreed with those obtained experimentally by Delgado, A., 2008 and can be concluded that moving reference frame can be applied to solve flow fields of squeeze film damper. Numerical simulations of three-dimensional cases with an additional central groove on the squeeze film land were also performed to predict the effect of central groove on dynamic pressure profiles. Addition central groove reduces the pressures and forces generated by squeeze film damper. Simulation of squeeze film dampers using moving reference frame reduces the simulation time drastically.

DEDICATION

To my mother

ACKNOWLEDGEMENTS

TABLE OF CONTENTS

LIST OF FIGURES

Page

LIST OF TABLES

1. INTRODUCTION

Squeeze film dampers are used in the high speed turbo machinery industry and aerospace industries as a means to reduce vibration amplitude, to provide damping, to improve dynamic stability of the rotor bearing system and to isolate structural components. There is a need to reduce vibrations of the rotor in rotating machinery as it has drastic effects upon the machinery parts. A squeeze film damper consists of a fixed journal, bearings on the outer layer of the journal and housing. The clearance between the journal and housing is filled with lubricant that is supplied at constant external pressure. The whirling motion of the journal, due to imbalance forces, generates pressure inside the lubricant film which, in response to these pressure forces, produces the damping forces that reduce the vibrations of the rotor. The lubricant *film* in between the journal and housing is *squeezed* to produce this damping reaction force; that is why they are called *squeeze film dampers.*

There are several aspects of squeeze film dampers that need to be investigated to predict their performance. Cavitation and Design parameters are particularly important. Ideally the performance of the squeeze film damper would be best if there are no cavitation affects in the lubricant film, since cavitation hampers their performance. Different types of cavitation occur in squeeze film dampers: vapor cavitation, gaseous cavitation and oil- air mixture cavitation.

This thesis follows the style of *Journal of Tribology.*

Vapor cavitation occurs due to formation of vapor bubbles at low pressures while gaseous cavitation can be due to air entrainment at low speeds, low supply pressures, or due to improper end sealing. Oil air mixture cavitation is due to the mixing of air bubbles in lubricant film, forming an oil air mixture with a certain percentage of dissolved air in it. The effects of cavitation were included in previous studies but effective and accurate models were not used for prediction of squeeze film dampers performance under different cavitation modes.

The effect of different design parameters were not studied thoroughly as earlier researcher's relied more on experimental methods than on numerical methods. Few of them used numerical investigation but the methods they used are either time consuming or complicated. Experimental investigation of squeeze film dampers for design parameters is very expensive. With faster computers being developed and Computational Fluid Dynamics (CFD) commercial software such as Fluent, simulation of prototypes through CFD has become relatively cheaper. Therefore, the method of investigation has been switched to simulation of squeeze film dampers through CFD commercial software. Researchers have also studied the suitability of applying CFD in general, but they again include simple, unsteady and time consuming models for solving the time dependent flow field of squeeze film dampers.

The present study investigated the feasibility of applying a steady state solver, which is computationally less expensive, for analyzing the flow field inside the squeeze film dampers, the behavior of dynamic pressure profiles at different operating conditions, and the effect of a central groove on dynamic pressure profiles. To verify the

applicability of a steady state solver for solving flow field inside the squeeze film dampers, simulation results of a 3D case which is similar to the one experimentally studied by Delgado, A., 2008 are compared. The effect of the central groove on the squeeze film land at different speeds was also analyzed. The results of each simulation were analyzed in TecPlot.

2. DESCRIPTION OF SFD CONFIGURATION

A Squeeze Film Damper has a non rotating journal mounted on ball bearings and a stationary outer housing surrounding it. The rotating motion of the journal is constrained by a squirrel cage and the gap between the journal and housing is filled with lubricant as shown in Figure 1. As the journal whirls or oscillates due to forces of imbalance, reaction forces are developed in the lubricant film. These reaction forces developed in the lubricant film damp the amplitude of journal vibrations. The governing equation based on Reynolds equation in polar co ordinates is given by

$$\frac{\partial}{R\partial\theta}\left(h^3\frac{\partial P}{R\partial\theta}\right)+\frac{\partial}{\partial z}\left(h^3\frac{\partial P}{\partial z}\right)=12\mu\frac{\partial h}{\partial t}+\rho h^2\left(\frac{\partial^2 h}{\partial t^2}\right)$$

where P is the dynamic pressure of the fluid film and h is the film thickness. Many solutions based on this equation have been proposed but they do not predict the forces accurately. Hence, a model for computational simulations is prepared.
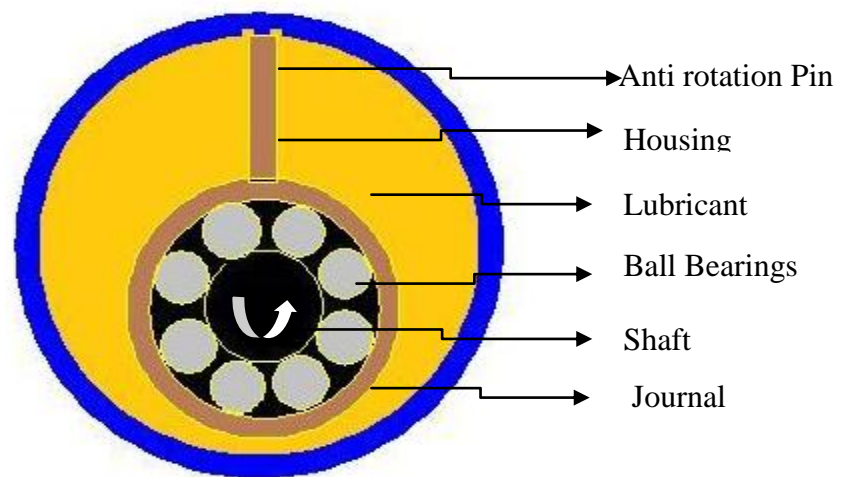
Figure 1: **Squeeze film damper**

Two general configurations were considered. The first was a journal with a smooth surface as investigated experimentally by Delgado, A., 2008 and depicted in Figure 2. This SFD was modified to place a groove circumferentially around the journal as depicted in Figure 3. Several grooves cross sectional areas and aspect ratios were considered. This groove is added to reduce the damping of the SFD.
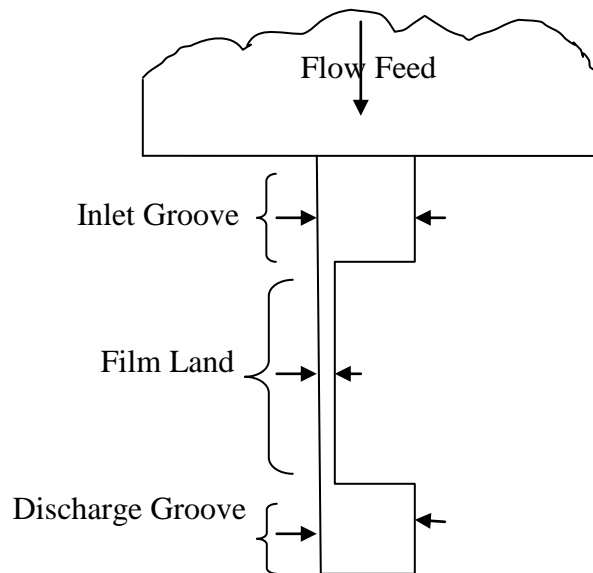
Figure 2: **Squeeze film land without central groove**
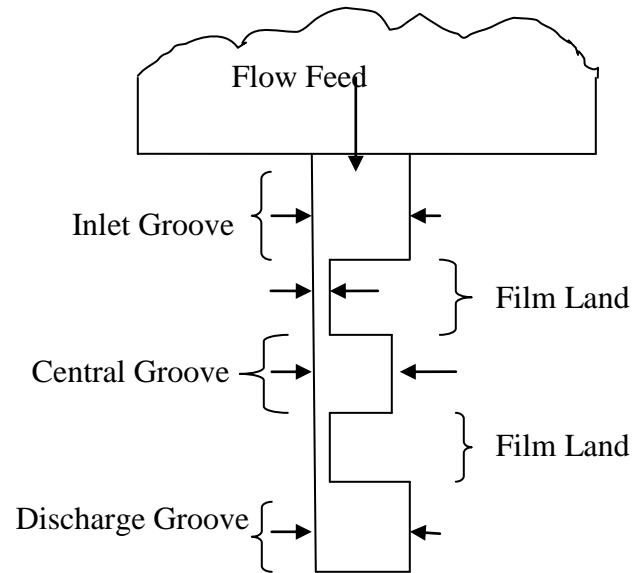
Figure 3: **Squeeze film land with central groove**

Any general force balance equation is of the form

$$M\ddot{x}+C\dot{x}+Kx+F=0$$

where M, C and K are inertia, damping, and stiffness coefficients.

In Squeeze Film Dampers since the static displacement is absent the stiffness coefficient is zero reducing the force equation to:

$$M\ddot{x}+C\dot{x}+F=0$$

The same equation can be represented in matrix form as

$$\begin{pmatrix} F_x \\ F_y \end{pmatrix} = -\begin{pmatrix} C_{xx} & C_{xy} \\ C_{yx} & C_{yy} \end{pmatrix}\begin{pmatrix} v_x \\ v_y \end{pmatrix} - \begin{pmatrix} M_{xx} & M_{xy} \\ M_{yx} & M_{yy} \end{pmatrix}\begin{pmatrix} a_x \\ a_y \end{pmatrix}$$

F_x – Force in X direction

F_y – Force in Y direction

C_{xx}, C_{yy} - Direct viscous Damping Coefficients

C_{xy}, C_{yx} - Cross-coupled viscous Damping Coefficients

M_{xx}, M_{yy} – Direct Fluid Inertia Coefficients

M_{xy}, M_{yx} - Cross-coupled Fluid Inertial Coefficients

Cross coupled force coefficients are due to motion perpendicular to the direction of the force.

The dimensions of inlet, discharge and central groove considered in this study are as follows:

Rotor radius – 63.5mm

Stator radius– 63.627mm

Eccentricity between stator and rotor – 0.074mm

Inlet groove clearance – 78c

Length of Inlet groove – 6.35mm

Discharge groove clearance– 31c

Length of Discharge groove – 4.1mm

where c is the clearance between the stator and the rotor and is 0.127mm.

The dimensions are from San Andres, L., 2008.
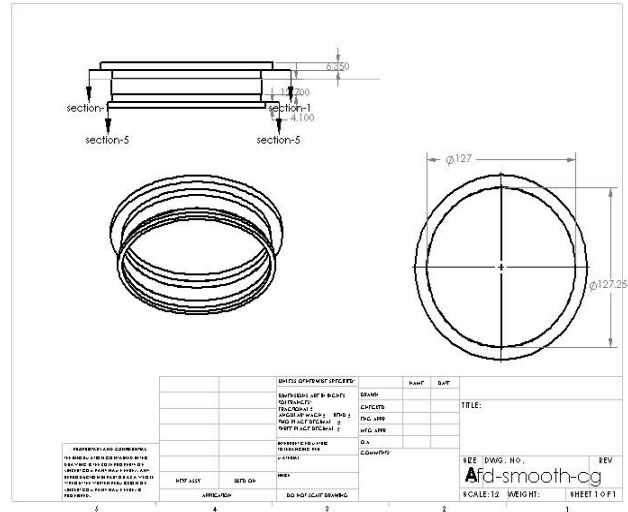
Figure 4: **Different views of squeeze film damper**

Central groove clearance varies from 0.5mm to 4mm and its length varies from 6.35mm to 12.7mm. Simulations are run to determine influence of dimensional parameters on Squeeze Film Damper performance. Different configurations of squeeze film dampers are prepared with several combinations of central groove dimensions. Three different views of the squeeze film damper with central groove and its dimensions are shown in Figure 4.

3. LITERATURE REVIEW

Zeidan, F., San Andres, L., and Vance, J., 1996, present the history of squeeze film dampers. Squeeze film dampers which were earlier used as a band aid solution are treated as excellent tools in reducing the amplitude of vibration in turbo machinery. The performance of a squeeze film damper and prediction of force coefficients has improved over the years. Proper design and usage of squeeze film dampers are very important for effective and optimum damping of vibrations and for increased bearing life. If the dampers are improperly designed, the system becomes over damped and acts as a rigid support. The low stiffness coefficients obtained through squeeze film dampers are the reason for its wide usage in turbo machinery. They gave insight into further research of SFD by providing the parameters that need to be investigated.

3.1   Experimental Studies on Squeeze Film Dampers

Vance, J., and Kirton, J., 1975, studied the hydrodynamic response of squeeze film dampers with end seals. They compared these results with "short bearing" and "long bearing" theories based upon Reynolds equation. As the end seals restrict axial flow, the long bearing theory can be applied; therefore comparison between theoretical and experimental results becomes appropriate. Reynolds equation used in this paper for comparison is founded on the assumption that the flow is laminar and neglects inertia terms. In reality the flow in rotor bearings is transient or turbulent in nature and inertia terms have an effect upon damper performance. This paper discusses the results of four different cases experimentally investigated with centered orbit and off centered orbit, both using SAE 10(light viscosity) oil and SAE 50 oil. The deviation of experimental

results from long bearing theory and non linear behavior of the dampers is explained based upon the fact that flow is either transient or turbulent in nature and also due to assignment of incorrect boundary conditions. This necessitates inclusion of a proper turbulent model for accurate prediction of squeeze film damper performance.

Zeidan, F., and Vance, J., 1990b, explain the difference between cavitation in a normal journal bearing and the squeeze film damper. With aid of high speed motion pictures, they observed five distinct regimes of cavitation and their characteristics which were distinguished with different pressure curves. The mode of cavitation and magnitude of damping coefficients depends upon several factors such as inlet supply pressure, eccentricity, type of sealing and also on journal speeds. In Zeidan, F., and Vance, J., 1989 and Zeidan, F., and Vance, J., 1990a, they discussed two types of cavitation in detail, gaseous and vapor cavitation. When both vapor and gaseous cavitation occur together, the severity of vapor cavitation is reduced which eliminates the overshoot of positive peak pressure. At higher speeds, gaseous cavitation splits into smaller groups of bubbles thus forming an oil-air mixture. Gaseous cavitation reduces the load capacity of the damper as the gaseous mixture compresses, shrinks in size and persists in the high pressure region. In their papers they also discussed air entrainment effects on coefficients of SFD. As the journal rotates at high speeds, air enters the squeeze film damper and bubbles are formed. These air bubbles are compressed due to the high pressures inside the film, forming a compressible mixture. However air bubbles, which are formed in negative pressure region, collapse as soon as they are subjected to increase in pressure; therefore they do not affect the positive pressure region. Air entrainment

decreases hardening effects and increases the non linear nature of the force coefficients. They also observed that the damping coefficients of SFD decrease with increase in eccentricity of the journal, because at higher eccentricities the lubricant becomes compressible due to air entrainment. One of the ways of eliminating Cavitation is by increasing the supply pressure. Their papers helped me choose a type of cavitation for the physical conditions of the SFD in my research.

Feder, E., Bansal, P., and Blanco, A., 1978, investigated the forces produced by squeeze film damper when following circular centered orbits and compared them with theoretical results from long bearing theory. Mechanically controlled orbits were used to generate forces in the squeeze film dampers which were moving in circular centered orbits. The important part of this investigation was to study the dynamic forces developed in the squeeze film damper between 180 degrees and 360 degrees, i.e, fully cavitated position to no cavitation position. It was observed that the inlet pressure and cavitation pressure have an effect on damper generated forces. Between 180 degrees to 360 degrees an increase in inlet pressure will increase circumferential pressure, damper forces, and decrease the stiffness force. As 360 degrees is reached, increase in inlet pressure has no effect on the pressure distribution. This paper demonstrates the general trend and the dependence of output parameters on input parameters. Thomsen, K., and Andersen, H., 1974, gave some quantitative results on damping coefficients generated when squeeze film dampers are used for controlling the rotor amplitude. These damping coefficients are obtained over a range of frequencies and for different film thicknesses and oil viscosities. Transmitted force coefficients and velocity of the sleeve are

measured directly from experiments using strain gauges. For practical purposes the results are in good agreement with theoretical results obtained from lubrication theory. They provide the Range of the damping forces produced by SFD.

El-Shafei, A., 1993, A discussed the new concept hybrid Squeeze Film Dampers which can act as a short damper as well as a long damper when required. Open ended Squeeze Film Dampers act as short dampers and tightly (end) sealed Squeeze Film Dampers act as long dampers irrespective of their lengths. This change in characteristic of damper is controlled using an adaptive controller which controls the ring seal position. He used the concept that the long damper has flow dominantly in the circumferential direction while the short damper has flow dominantly in the axial direction; therefore the pressure gradient is in the circumferential and the axial direction respectively. Long dampers attenuate the vibrations of a rotor effectively while short dampers reduce the force transmitted to the engine effectively. Long dampers does not exhibit a jump resonance phenomenon but due to inertial mass effect they exhibits additional critical speed while short dampers exhibit the jump phenomenon. Both the dampers characteristics are combined in a hybrid damper to provide effective damping throughout the operating speed. This hybrid damper is tested on Bently Nevada Rotor kit to prove the theoretical predictions and effectiveness. Delgado, A., 2005, conducted experiments to determine mechanical parameters influencing Squeeze Film Dampers with end seals. The damping of the entire system includes dry friction in the mechanical seal, squeeze film land and from supporting structures. Static stiffness is obtained from static load tests without end seals in place, dry friction force which is included as

equivalent viscous damping coefficient is obtained from an energy balance method. The squeeze film damping coefficient is obtained from equating total work done to energy dissipated by each type of damping. The results show that the damping coefficients are higher at low frequencies and low amplitudes and these were in good agreement with short bearing model results. The results also show that the end seal effectively prevents air entrapment into the squeeze film land. This paper also provides dependence of different output parameters on input parameters.

3.2   Numerical Studies on Squeeze Film Dampers

Feng, N., S, and Hahn, E., J, 1986, developed a solution for Reynolds equation which can accommodate arbitrary density-pressure and viscosity-pressure relationships. The solution for Reynolds equation is valid for bearings with length to diameter ratios less than 0.25. They compared these solutions with several theories which adapted different incompressible fluid cavitation models such as π model, 2π model and pressure truncation model over a wide range of operating conditions; they seem to agree very well. Assumptions related to the thermal process, saturation pressure, operating conditions etc do not affect the results. Xing, C., 2009, analyzed different end seals and their effect on dynamic pressures and forces transmitted by a squeeze film damper. They performed numerical simulations of these models with available finite volume commercial codes. They found that for a piston ring seal, the variation of pressure and dynamic force coefficients decreases as the number of grooves increase. They observed the same trend with partially sealed damper using serrated piston rings. With a fewer number of grooves the pressure and force coefficients become distorted. The magnitude

of variation of the radial and tangential forces decreases with an increase in number of grooves. The results also confirmed that seal clearance should be much less than damper clearance for the damping coefficient to increase. The damping coefficients also increase with an increase in groove length. Quantification of these variations, which can be used to predict the operating range of squeeze film dampers, is not provided. Delgado, A., 2008, performed analysis of SFD and oil seals using fluid flow analysis which divides multiple grooves into regions of constant clearance; this is called linear fluid inertia model. An effective groove clearance is defined. Boundary conditions used for the SFD are discharge pressure conditions measured in experiment. Both axial and circumferential pressure variation is considered and it was observed that axial pressures are high in grooved regions. It was seen that pressures generated in grooves and plenums were of inertial nature. It was also observed that predicted force coefficient is a function of groove depth. Comparisons of experimental and predicted results show good agreement for a narrow range of effective groove clearance.

Gertzos, K. P., Nikolakopoulos, P. G., and Papadopoulos, C. A., 2008, applied CFD for analyzing hydrostatic, hydrodynamic, hybrid journal bearing operating conditions and squeeze film dampers, and they compared these solutions with different standard codes already established. The CFD simulation results of hydrostatic and hybrid operating conditions were in good agreement with existing codes. Moving grid method and conjugate heat transfer methods were included for analysis of damper characteristics and squeeze film dampers. The nodes can be moved in the desired profile with the help of user code written in FORTRAN. Simulation with CFD proved to be

time consuming but this procedure is more efficient for complex geometries. Chen, P., and Hahn, E., J, 1998, observed that CFD software can be used for handling steady state hydrodynamic lubrication problems such as slider, step, journal bearings and squeeze film dampers under constant unidirectional or rotational loading. A limited numbers of cases were considered in this damper study .Validation of results for long and short bearings are done against the solutions available from Reynolds equation. Results from CFD simulations confirmed the radial pressure distribution and neglection of viscous terms in Reynolds equation. The results also suggest that for squeeze film dampers exhibiting circular orbits the temporal inertial coefficient and convective inertial coefficient have opposite effects, therefore that the net effect of inertial terms is negligible but the inertial forces should not be neglected. The impact of inertial force on load capacity is directly proportional to the Reynolds's number. These papers together prove that CFD can be applied to solve for flow fields of SFD.

Gertzos K.P., Nikolakopoulos P.G., and Papadopoulos C.A., used lubricants which behave like Bingham fluids in journal bearings. Analysis of three dimensional models using Bingham fluids was performed using commercial CFD software called Fluent with dynamic mesh technique. Journal bearing performance characteristics are obtained for various L/D bearing ratios and dimensionless shear stress (T_o). The results obtained from CFD simulations are in good agreement with experimental and theoretical results investigated previously. They observed that as the eccentricity increases, the core formation moves from inlet to outlet and a floating core starts appearing. The effect of yield stress (T_o) on a journal bearing is very small for low eccentricity ratios. The load

carrying capacity and film pressure is higher when using Bingham fluids than when using Newtonian fluids. Final results were presented in the form of charts which can be used by any designer. Terdsak, N., 2011, performed numerical study on two dimensional squeeze film dampers using commercial software called FLUENT for both single phase and multiphase flow models, with the journal taking linear orbits. For single phase flow, journal amplitudes of 0.002, 0.001, and 0.0005mm in a nominal clearance of 0.127 mm and journal frequencies of 10, 50, and 200Hz were analyzed. It was observed that maximum pressures and maximum forces vary directly with amplitude and frequency of the journal. The multi phase flow was modeled with amplitude of 0.002mm and frequencies of 10, 50, and 100 Hz. Operating pressures of 0.001, 0.01, 0.05, 0.1, 0.5, 1, 10, 50, and 100MPa were used for the study. When the operating pressure is close to the vapor pressure of the lubricant, the squeeze film is filled with vapor. As the operating pressure increases Liquid fraction decreases. It was observed that the cavitation affects the force exerted by squeeze film dampers and this effect can be reduced by increasing operating pressure.

Milind, K., 2011, Khandhare examined the feasibility of applying commercial CFD (Fluent 12) software for solving squeeze film dampers. A time dependent solver called dynamic mesh model with user defined functions was used to produce the whirl motion of the journal. A Mixture model for multiphase flows along with Singhal Cavitation effect in Fluent was used to the simulate squeeze film damper. Both two dimensional and three dimensional cases were simulated with variation in percentages of dissolved air. The results are compared with experimental results of a 5 mil, 50 HZ

frequency case by Delgado, A., 2008. The results were in general in good agreement with experimental results but pressures predicted in the cavitation region were slightly higher than the experimental values. The flat portion of the pressure curve and slow increase in pressure observed is attributed to ingestion of air and gaseous cavitation in the squeeze film damper. Terdsak, N., 2011, and Milind, K., 2011, used dynamic mesh model to solve for flow fields of SFD which is very time consuming and computationally highly expensive. Therefore in the present study feasibility of applying steady state solver was studied.

4. OBJECTIVE

The objectives of the work in this thesis are:

1. To demonstrate that the moving reference frame model (steady state solver) in Fluent 12.1, a CFD commercial code, can be used to simulate the flow field inside Squeeze Film Dampers. This will allow replacing a 3D time dependent solution technique with a 3D steady state solution technique resulting in a significant reduction in computer usage.

2. To establish an optimum grid size for 3D model and required solvers in Fluent for simulating the flow field in squeeze film dampers.

3. Simulate the case that was experimentally studied by Delgado, A., 2008, and additional cases with different central groove dimensions.

4. Simulate the case experimentally studied by Delgado, A., 2008, and an additional case with central groove of smallest clearance at higher whirling speeds of 100Hz.

Experimental analysis of squeeze film dampers with different geometries is expensive and becomes very cumbersome. Dynamic meshing models and user defined functions can be time consuming. So if the moving reference frame can be established as a feasible model for solving squeeze film dampers then the simulation time reduces drastically. The cavitation treated in this work is only gaseous cavitation, which includes dissolved air in the lubricant, since the vapor pressure of lubricant is not very low at low speeds. The SFD configurations used in this work are based upon Delgado,A's 2008, experimental facility with additional central grooves of different dimensions.

5. METHODOLOGY

A three-dimensional model, which has the same dimensions as that used by Delgado, A., 2008's, experimental model, was used to establish if the moving reference frame (MRF) model in Fluent 12.1 can be used. The model has a journal diameter of 127mm with a clearance of 0.127mm and an eccentricity of 0.074mm. The length of the squeeze film land is 25.4mm and has a whirling frequency of 50 Hz. Any model solved using CFD has to be divided into a number of small elements so that the partial differential equations for each parameter can be solved numerically in each element individually to acquire the solution for the entire model. To avoid highly skewed elements and to use finite difference method for solving partial differential equations, the model has to be meshed structurally.

The mesh was generated using the mesh generation tool GAMBIT 2.4.6 with mapped mesh and hexahedral structured mesh tools for two-dimensional and three-dimensional models respectively. The two dimensional cases of various grid sizes were simulated with a CFD commercial code Fluent 12.1 to establish an optimum grid size of 1440 nodes along the circumference and 45 nodes across the clearance, where the results do not depend on the grid size larger than this any further. This is called a grid independent study and a grid size of 1440×45 was established from this study. Bi-exponential compression is used across the clearance to compress the grid in the radial direction toward the walls so as to accommodate for the boundary layer effects. One hundred nodes along the length of the axis of the film land were used for grid generation in three-dimensional cases. Bi-exponential compression was used in all radial directions;

this makes a grid with a total of 10 million nodes. Due to the large mesh size, parallel processing mode with 8 partitions was used in Fluent 12.1.

A steady state solver in an absolute frame of reference was used to produce whirling motion of the rotor in this study. The working medium used in this study was VG 2 Mobil oil with a density of 800kg/m^3 and a dynamic viscosity of 0.0016kg/ms. The inlet pressure of 31kpa and the whirling speed of 50 and 100Hz were used as boundary conditions. The mixture model with 3 percent dissolved air in lubricant and the Singhal cavitation model were used to model multiphase flow with cavitation. Standard wall function is used foe boundary wall effects. Y plus of 30-300 is required by standard wall function, which is achieved by bi exponential compression in radial direction. The Pressure-velocity coupling SIMPLEC algorithm was used to solve the continuity equation and for the pressure discretization PRESTO scheme was chosen. The equations for density, momentum and kinetic energy were discretized with a second order upwind scheme while vapor and dissipation rate were discretized with a first order upwind scheme. Second order upwind scheme is used initially to discretize dissipation rate, but convergence could not achieved with second order upwind scheme even after using this scheme after several thousand iterations. Therefore first order upwind scheme is used finally. The Convergence criteria of 10^{-5} were used for all the parameters listed above. The PRESTO scheme and a second order upwind discretization were chosen as they provide the most accurate results for steady state solvers. The simulations (50,000 iterations) were run until steady state solutions were reached. Numerical simulations of

three-dimensional cases with an additional central groove on the squeeze film land were also performed to predict the effect of central groove on dynamic pressure profiles.

The results of the 5 mil, 50 Hz case were then analyzed in TecPlot at various sections of the squeeze film land but results at mid land section were used for comparison as experimental results are available at this section. The results of the 5 mil, 100Hz smooth squeeze film damper case were compared with the results of the 5 mil, 50 Hz case to study the effect of higher whirling speeds on squeeze film dampers. The effect of the central groove upon dynamic pressure profile is studied by comparing the results of SFD with a central groove on its film land to SFD without any central groove on it. For better analysis the flow field section was enlarged in TecPlot with a coordinate transformation technique. The following equations are used to evaluate X mod and Y mod. The plot of X mod vs Y mod produces an enlarged section.

$$X' = \sqrt{X^2 + Y^2} \tag{1}$$

$$Y' = \tan^{-1}\left(\frac{Y}{X}\right) \tag{2}$$

$$\text{Mod\_Radius} = X' - 0.0632 \tag{3}$$

$$X \text{ mod} = \text{Mod\_Radius} \times \cos(Y') \tag{4}$$

$$Y \text{ mod} = \text{Mod\_Radius} \times \sin(Y') \tag{5}$$

6. RESULTS AND DISCUSSION

6.1 Grid Independent Study

Usually, there is a need to establish the grid independence of the results produced by computational methods (CFD) i.e. results of the simulation should not depend on the size of the mesh of the model. It this thesis, the steady state (Moving Reference Frame) method is used to solve for the dynamic pressure distribution of squeeze film dampers. With low clearances as in squeeze film dampers, using a steady state solver necessitates a high density mesh in the clearance to provide accurate results. Two-dimensional models are used for the grid independent study instead of three-dimensional models as high density mesh in three-dimensional models makes them computationally exhaustive. The grid independent study considered orbit rotating at 50Hz.
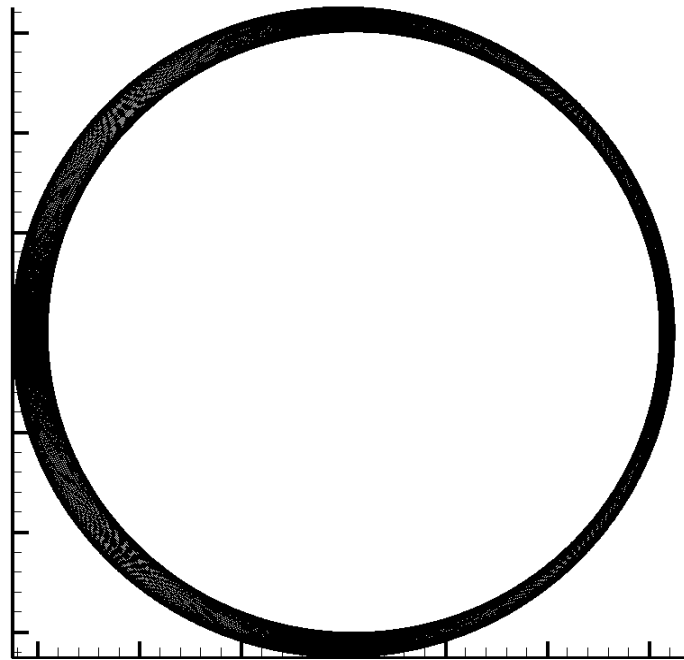

Figure 5: **2D mesh of 1440 X 45**

A coordinate transformation is used in TecPlot to enlarge the clearance. Figure 5 shows 2-D grid of SFD. To establish the correct grid size, initially the number of nodes in the radial direction was kept constant at 45 and the circumferential nodes were decreased from 4320 to 2880 and from 2880 to 1440. Table 1 shows that the percentage change in total forces developed in the squeeze film damper are negligible with change in number of nodes in the circumferential direction. 720 nodes around the circumference were not enough for the solution to develop. Hence, a grid size of 1440 was used in the circumferential direction. Next, the number of nodes in the circumferential direction was fixed at 1440 and the radial number of nodes was varied from 30 to 45. A significant difference in forces up to 10% was observed, and after 200000 iterations the differences came down to negligible values. Then the mesh size in the radial direction is increased from 45 to 60. An Initial difference in forces of 5% was observed during first 5000 iterations but later they came down to negligible values as the number of iterations increased to 50000. So the mesh size in radial direction in the clearance is fixed at 45. Hence the grid size of 1440×45 is used for simulation of Squeeze film dampers with bi exponential compression all over the grid in the radial direction to capture phenomenon close to the wall (boundary layer phenomenon). This compression allows the y+ values to be less than 300, which is required by the wall function and also without being excessively fine in the clearance region. When bi exponential compression with a factor 0.75 is used, the numbers of nodes in the center are fewer than closer to walls. Table 1 indicates the percentage changes in force developed in the squeeze film dampers for different grid sizes:

Table 1: Grid independent study for azimuthal and radial nodes

| FORCE(N) on Rotor					4320 vs 2880	60 vs 45	2880 vs 1440	45 vs 30
1440 X 30	1440 X 45	4320 X 45	2880 X 60	2880 X 45	A_err (%)	R_err (%)	A_err (%)	R_err (%)
3906	3608	3930	3569	3787	4	6	-5	-8
7139	6688	7222	6691	6986	3	4	-4	-6
9791	9240	9889	9258	9603	3	4	-4	-6
11984	11361	12064	11377	11756	3	3	-3	-5
13795	13125	13837	13126	13529	2	3	-3	-5
15277	14584	15267	14560	14975	2	3	-3	-5
16447	15763	16374	15709	16120	2	3	-2	-4
17290	16662	17158	16585	16961	1	2	-2	-4
17794	17275	17621	17183	17498	1	2	-1	-3
17981	17608	17793	17519	17748	0	1	-1	-2
17894	17692	17707	17622	17746	0	1	0	-1
17582	17560	17405	17524	17529	-1	0	0	0
17095	17251	16931	17256	17141	-1	-1	1	1
16489	16805	16335	16859	16624	-2	-1	1	2
15824	16267	15677	16367	16029	-2	-2	1	3
15162	15681	15019	15825	15409	-3	-3	2	3
14559	15095	14422	15273	14818	-3	-3	2	4
14055	14554	13929	14753	14299	-3	-3	2	4
13676	14091	13565	14298	13880	-2	-3	1	3
13425	13727	13334	13930	13577	-2	-3	1	2
13291	13431	13221	13657	13385	-1	-2	0	1
13254	13308	13204	13479	13293	-1	-1	0	0
13292	13238	13258	13385	13282	0	-1	0	0
13378	13237	13357	13362	13330	0	0	-1	-1
13492	13288	13481	13389	13416	0	0	-1	-2
13616	13373	13611	13455	13524	1	1	-1	-2
13735	13475	13732	13540	13639	1	1	-1	-2
13839	13582	13837	13637	13745	1	1	-1	-2
13924	13681	13922	13731	13839	1	1	-1	-2
13989	13769	13984	13817	13915	0	1	-1	-2
14032	13841	14025	13889	13974	0	1	-1	-1
14054	13895	14044	13946	14012	0	0	-1	-1
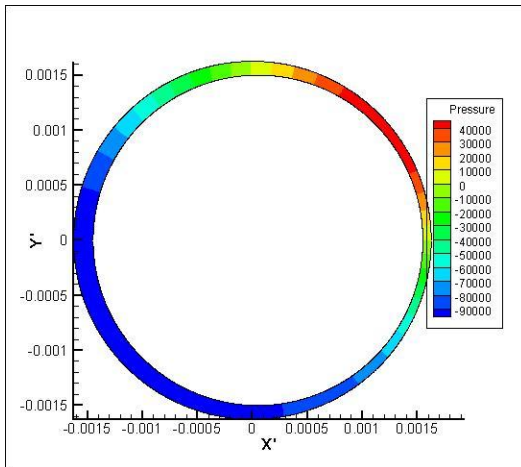
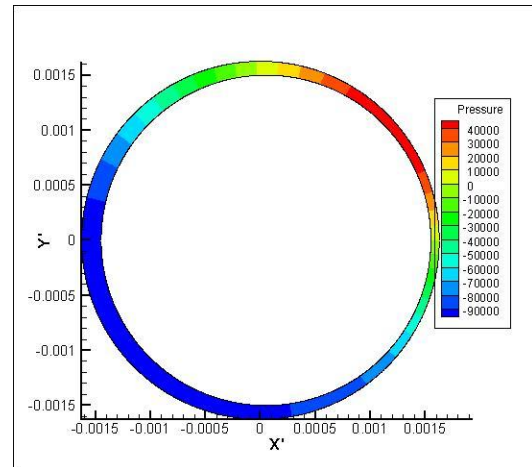**Figure 6: Pressure contour for 1440 X 30**

Figure 7: Pressure contour for1440 X 45
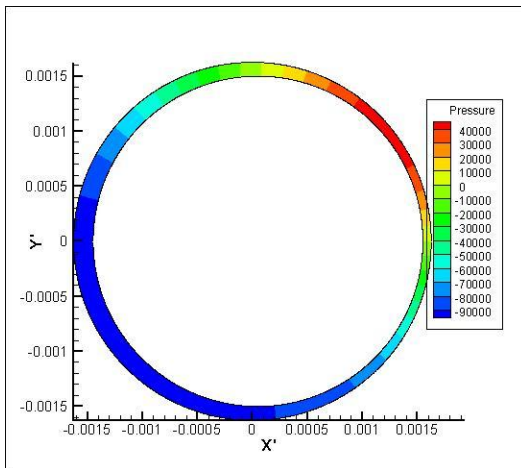

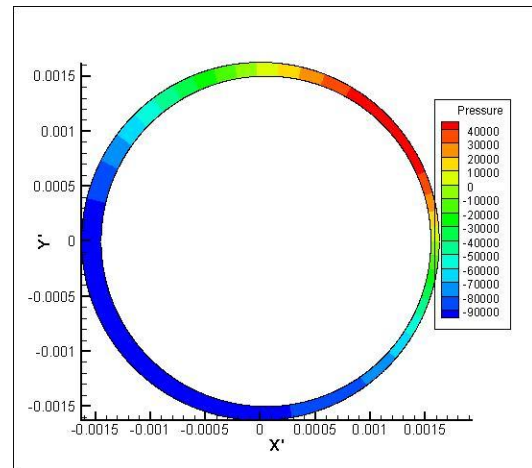**Figure 8: Pressure contour for 2880 X 30**

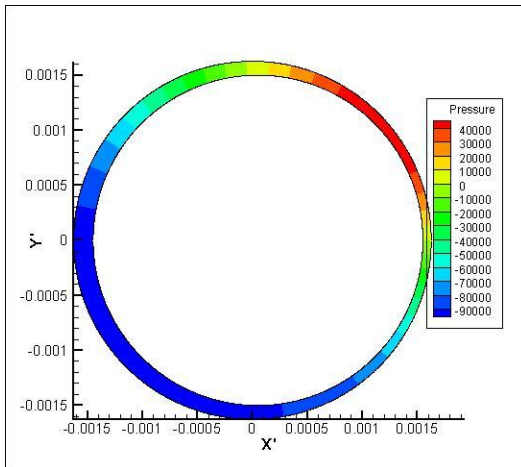

Figure 9: Pressure contour for 2880 X 45

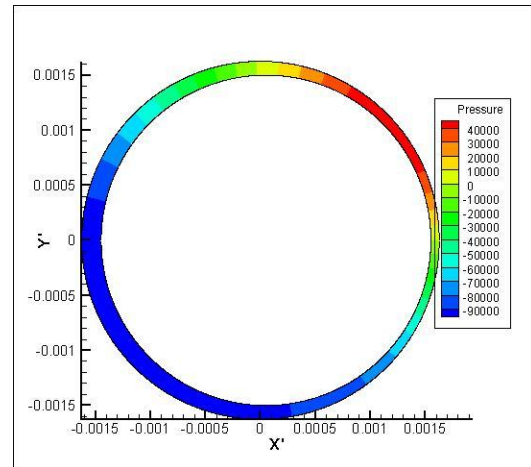**Figure 10: Pressure contour for 2880 X 60**

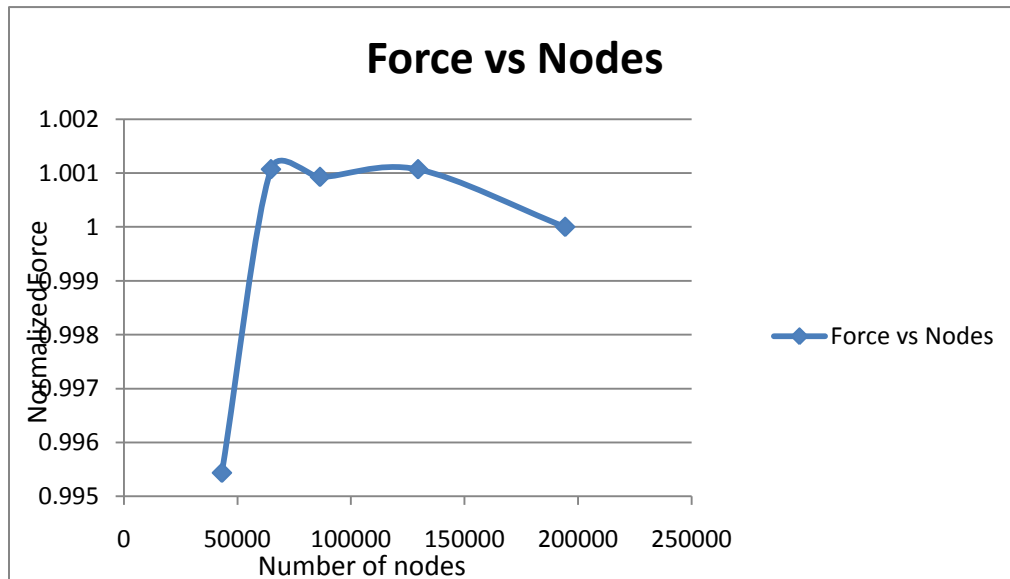**Figure 11: Pressure contour for 4320 X 30**

Figure 12: Normalized force vs number of nodes

Pressure contours are evaluated as the pressure distribution is the quantity of interest in this study. Figure 6 to 11 represent pressure contours after 200,000 iterations for different grid sizes. Figure 12 represents variation of force values with variation of grid size for grid independent study. The magnitude and position of the high and low pressure regions are the same for all the grid sizes. Pressure distributions are essentially

the same for all cases. The minimum clearance is located at Xmod = 0.0015 and Ymod = 0. The journal is rotating in counter clockwise direction at 50 Hz. These data confirm Reynolds assumption of negligible pressure variance in the radial direction. For grid independence in Z (third) direction, adaptive gridding method is used with Y plus as target. Adaptive gridding is done until Y plus of 300 is achieved; simulations are run until convergence of 10^{-5} is reached for all parameters. Starting gambit grid of eighty numbers of nodes in Z direction, hundred numbers of nodes is reached. This results in a total of 10 million nodes for a three dimensional model.
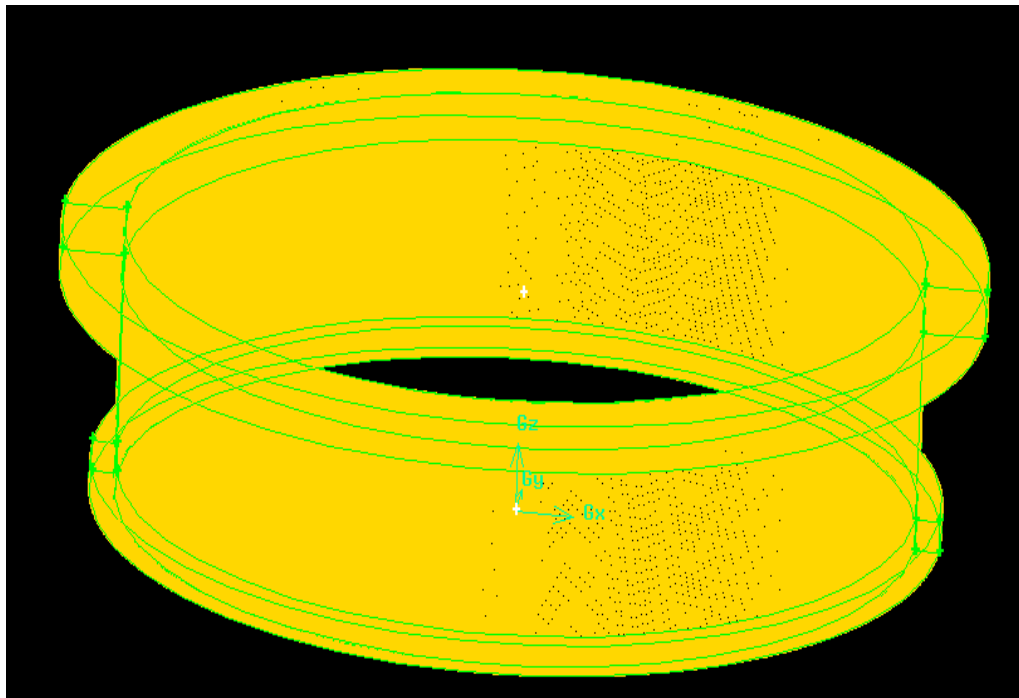

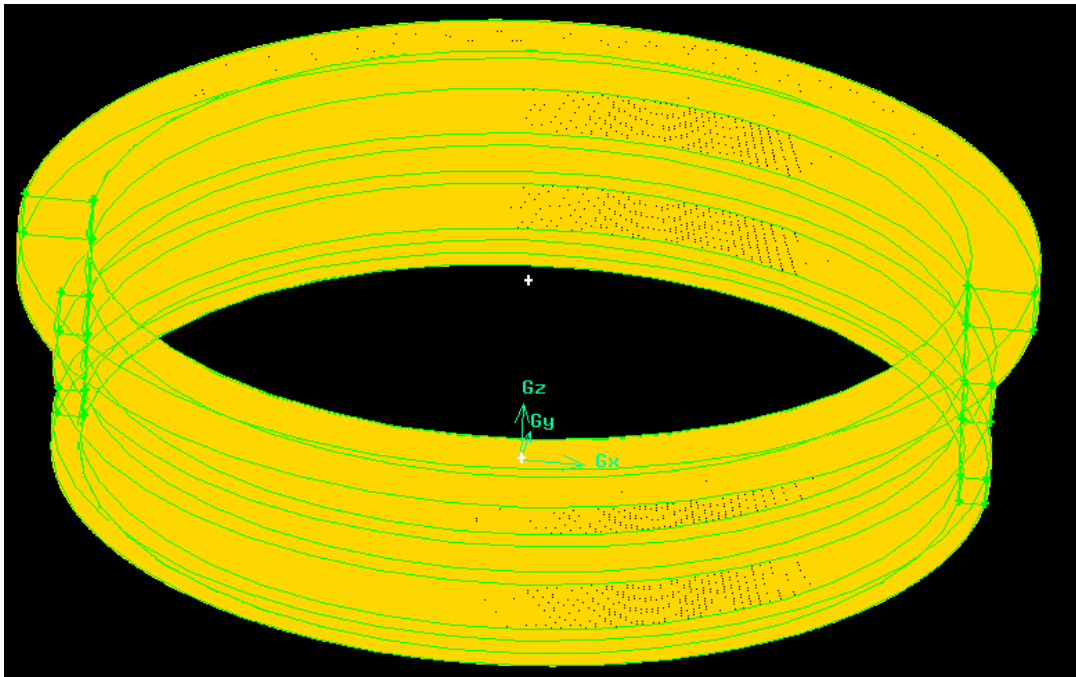**Figure 13: 3D grid of 1440 X 45 without the central groove**

Figure 14: 3D grid of 1440 X 45 with the central groove

6.2 Comparison of CFD and Experimental Results

The circumferential and radial grid size of 1440×45 is used for the three dimensional SFD models. One thousand four hundred and forty nodes are used in the circumferential direction of central groove, forty five nodes in the radial direction and hundred nodes are used in the axial direction of the squeeze film damper's land. Bi exponential compression is used in the radial direction for the inlet; discharge and central groove to assure an adequate numbers of nodes are present near walls to capture boundary layer effects. A high density mesh is necessary when using the steady state solver to accurately solve for dynamic pressures in three dimensional squeeze film dampers. Figures 12 and 13 show the high density three dimensional grid, without and with the central groove respectively.

Gambit 2.4.1 was used to create this model with a grid size of 1440 X 45 X 100. This grid was then imported into Fluent for simulation. Mobil Velocite 3 with 3% dissolved air was used as the working fluid with density = 800 kg/m^3, viscosity = 0.0016 kg/m-s (2 cSt), and vapor pressure = 1mmHg (0.1336 kPa). A pressure based steady state solver with absolute velocity formulation was used to solve the flow field. A pressure of 31Kpa was used as the inlet boundary condition, and both stator and rotor rotate at 314 rps in the clockwise direction which is equal to journal orbit speed. This motion of both rotor and stator simulates a circular orbit with the fluid remaining stationary. However, in the stationary reference frame, the fluid rotates in an anti clock wise direction with a speed of 314 rps. The results obtained from the simulation of this model are compared for the pressure with experimental results obtained by Delgado, A., 2008, at the center of the journal land. The data are presented in this figure as absolute pressure in bar and theta in degrees (0-360) on the Y and X axes respectively. Figure 14 shows that the trend of experimental pressure profile is closely followed but, with a slight shift to higher pressure values. This shift may be due to non inclusion of air entrainment effects in the film, which are present in the experiment, into the simulated CFD calculations. This air entrainment reduces the pressures since added gas increases the compressibility of the fluid mixture. Since the amount of air entrapped in lubricant is unknown, this shift can also be reduced by increasing the percentage of air dissolved in lubricant as it seen in Milind, K., 2011,'s thesis that as the percentage of dissolved air increases from 3% to 7%, the pressure values came down by 19%. The flat portion of the curve, which is due to cavitation (gaseous), is also predicted. This illustrates that the

steady state (Moving Reference Frame) method can be applied to solve flow fields of squeeze film dampers.

The pressure and velocity plots of the base case, without any central groove at mid section of squeeze film land, are shown in Figures 16-19. The velocities are presented in the moving reference frame coordinate system which is rotated in the clockwise direction. Comparison of tangential velocity in the stationary frame of reference and the moving frame of reference is shown in Figures 20 and 21. Figures 22-23 represent pressure and liquid fraction plots at section-1 which is 6.35mm from the inlet with red color indicating high pressure region and blue indicating low pressure region. Figures 24-25 represent pressure and liquid fraction plots at section-5 which is 4.1mm from bottom (outlet).
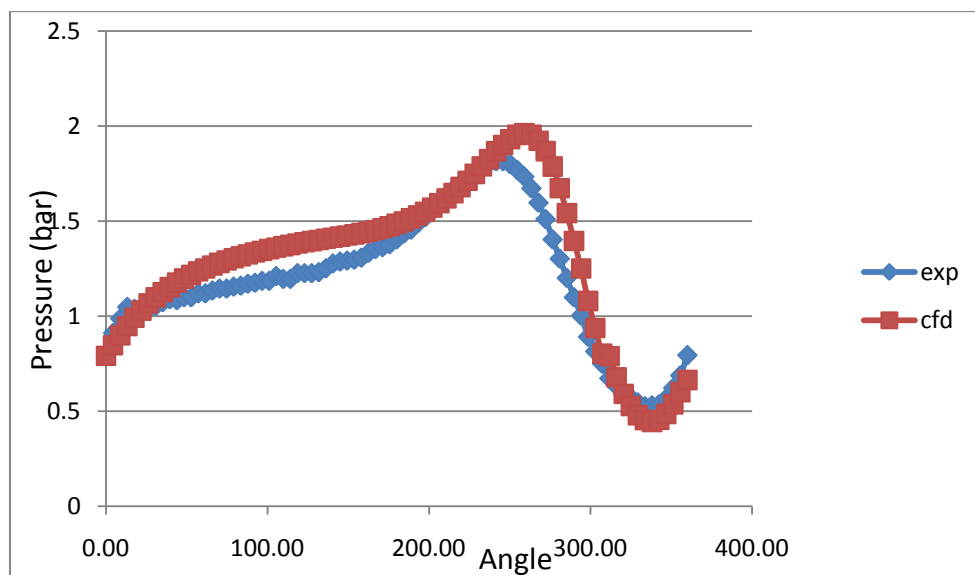

Figure 15: Comparison of experimental and CFD results for SFD operating at 50 Hz
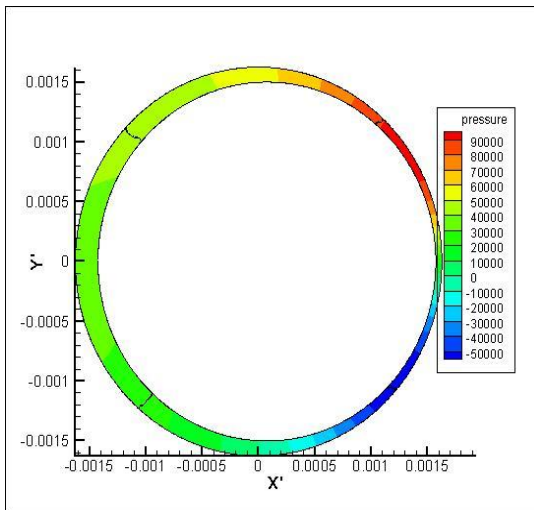
Figure 16: Pressure distribution for a section at mid land operating at 50Hz
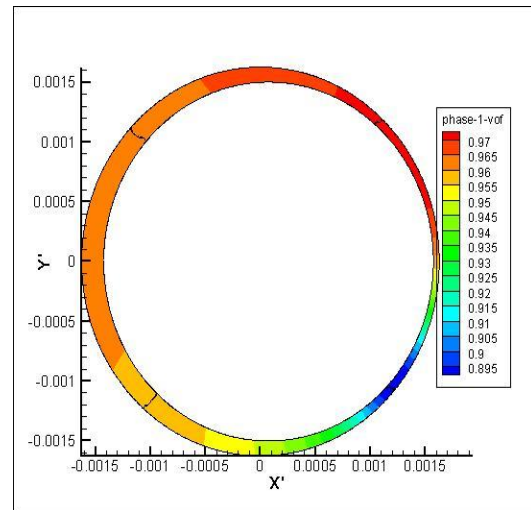

Figure 17: Liquid fraction distribution for a section at mid land operating at 50Hz
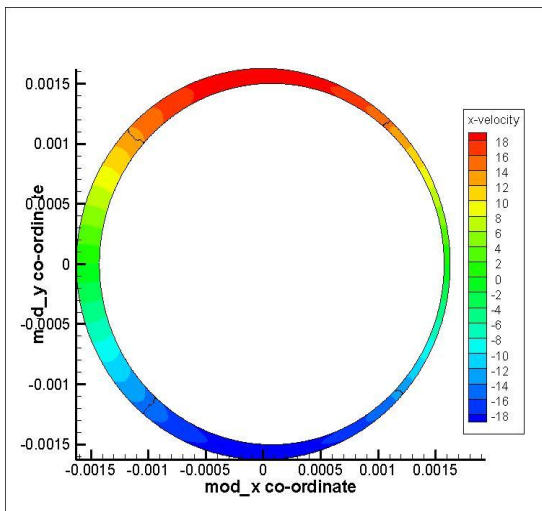

Figure 18: X velocity distribution for a section at midland operating at 50Hz in moving reference frame
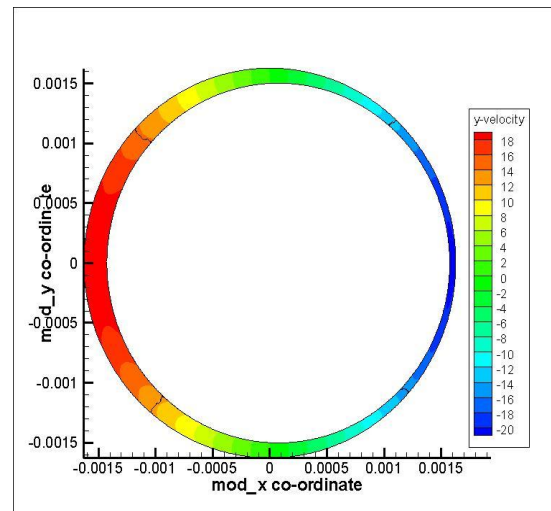

Figure 19: Y velocity distribution for a section at midland operating at 50Hz in moving reference frame
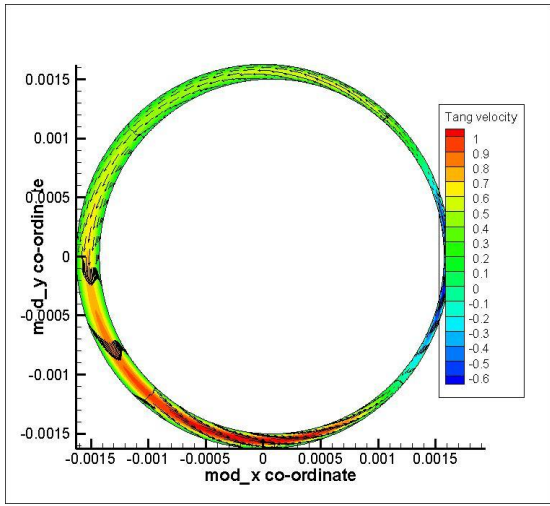
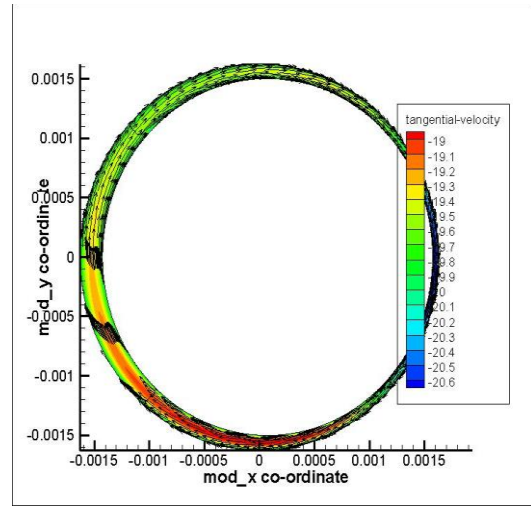Figure 20: Tangential velocity at 50 Hz moving reference frame

Figure 22: Tangential velocity at 50 Hz in stationary reference frame
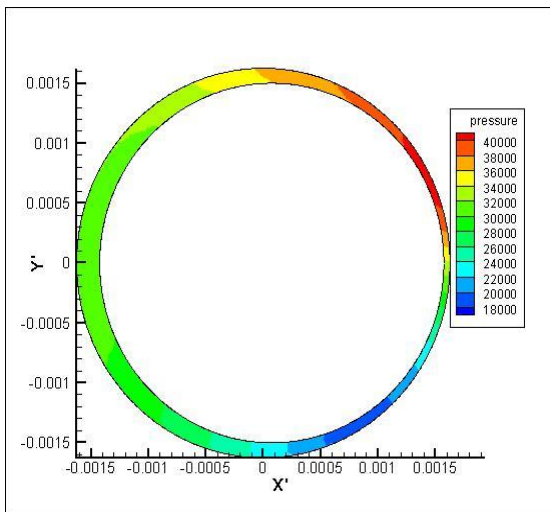

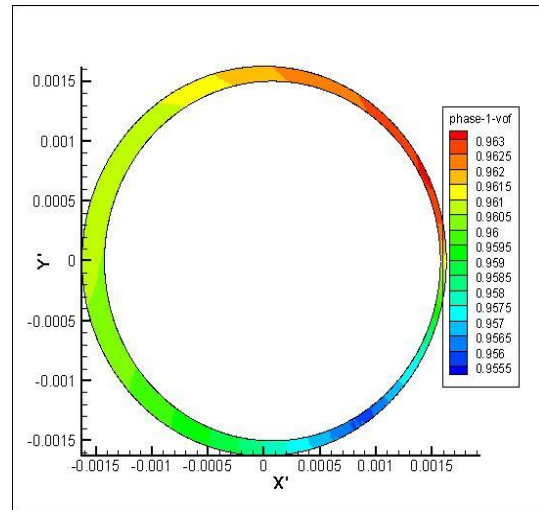Figure 21: Pressure distribution for Section-1 operating at 50 Hz
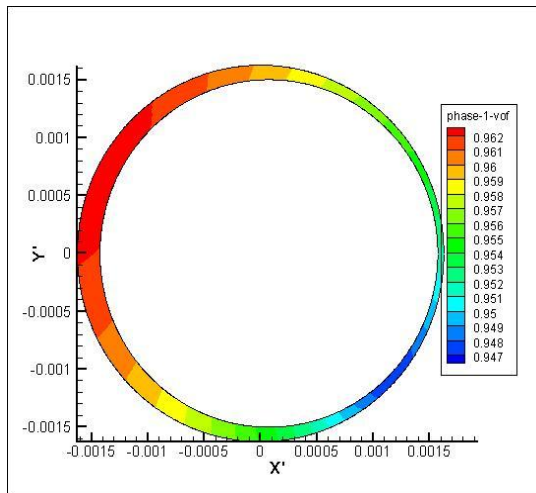

Figure 23: Liquid fraction at section-1 operating at 50Hz

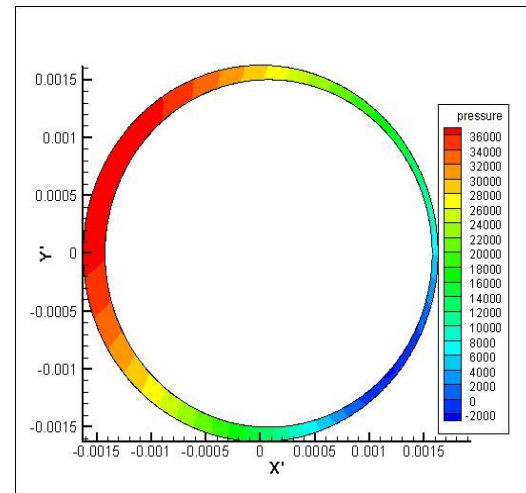**Figure 24: Pressure distribution for Section-5 operating at 50 Hz**

Figure 25: Liquid fraction at section-5 operating at 50Hz

From Figures 16-17 and 22-23 it can be seen that the pressure at mid land ranges from -50kpa to 90kpa while pressure at section-1 which is located at 6.35mm from the inlet is reduced to almost the supply value and has a range of 18kpa to 40kpa. Liquid fraction at mid land ranges from 0.897 to 0.97 while at the inlet (section-1) liquid fraction ranges from 0.955 to 0.963. This shows that the pressure and amount of vapor at the mid land region is higher than at the inlet or the outlet sections. The decrease in pressure from center of the land to inlet is also observed in journal bearings. It can also be seen that at the peak pressure highest liquid fraction also occurs, which is close to minimum clearance position. The pressure distribution in a finite length journal bearing is given by Equation 6 where z is measured from journal center land and theta is circumferential angle measured in counter clockwise direction from minimum clearance position. However the pressure distribution in a journal bearing is created by viscous drag (no journal orbit motion) and flow is assumed to be laminar. For the journal bearing operating under these conditions the maximum pressure would be $753,600 \text{N/m}^2$ as

compared to 196,254N/m^2 for the SFD. The maximum pressure developed in the journal is given by Equation 7 with C_p being 1:

$$P = \frac{3\mu\omega}{c^3}\left(\frac{\partial h}{\partial x}\right)\left(z^2 - \frac{l^2}{4}\right)\frac{\epsilon \sin\theta}{(1+\epsilon \cos\theta)^3} + P_o \tag{6}$$

$$C_{p=} \frac{Pc^2}{6\mu\omega R_c^2} \tag{7}$$

The squeeze film damper generates pressure by pushing the fluid around the circumference by the whirling motion of the journal. This difference in physical mechanism not only explains the difference in magnitude but also explains the occurrence of maximum pressure on the opposite sides of the minimum clearance. This is valid when the journal orbit rotation direction for SFD is same as for journal bearing in the stationary coordinate frame. Figures 26 and 27 show that the variation of pressure distribution with axial location at maximum and minimum pressure locations takes quadratic form just as in the case of journal bearings.
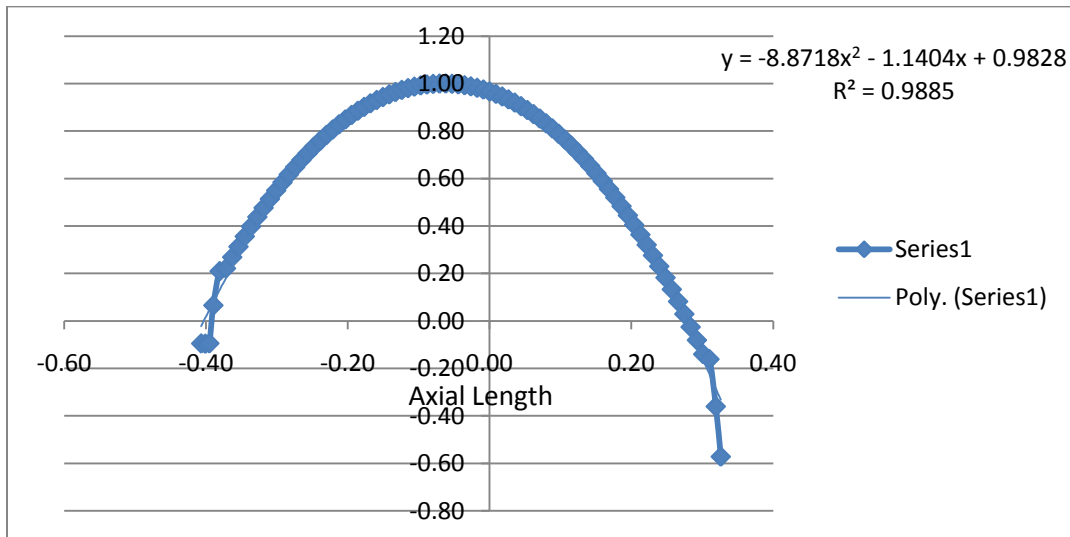

Figure 26: Pressure distribution along axial direction at minimum pressure location (50Hz)
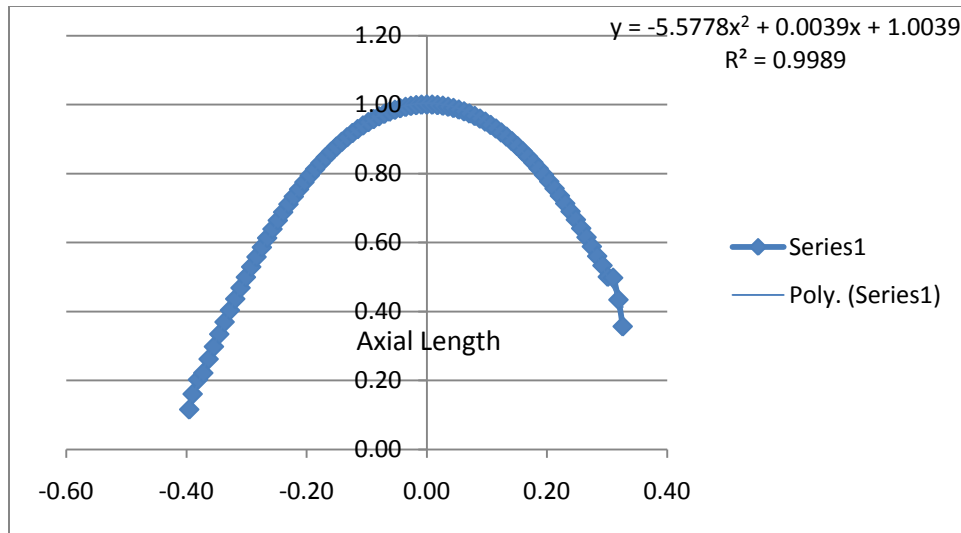
Figure 27: Pressure distribution along axial direction at maximum pressure location (50Hz)

Figures 18 and 19 represent X and Y velocity distributions at mid land section in moving reference frame coordinate system. The direction of velocity vectors (x-velocity and y-velocity) changes from clockwise in the moving reference frame to anti clockwise in the stationary reference frame when x and y velocity vectors are transformed using Equations 7 and 8 to represent actual velocities in stationary reference frame. The magnitude of the tangential velocity also changes when it is transformed using equation 6 to represent the absolute tangential velocity. This can be observed from Figures 19 and 20. These equations are as follows

Vmod_tangential = Vtangential + r x ω   (8)

Vmod-X velocity = Vmod_tangential x cos(Y′)   (9)

Vmod-Y velocity = Vmod_tangential x sin (Y′)   (10)

6.3 Variation of Operating Conditions

When the same configuration is run at 100 HZ orbit frequency, the dynamic pressure values generated in the squeeze film land at mid-section are almost double the values of that generated at 50Hz, but the position of occurrence of maximum pressure relative to minimum clearance position remained the same at both the speeds. This increment in pressure value can be attributed to higher turbulence, inertial forces and cavitation at higher speeds. From Figures 28 and 29 it can be seen that the minimum pressure values at higher speeds are more negative and are below atmospheric pressures causing large amounts of cavitation. The cavitation and increase in pressure values that occur in the squeeze film land are due to the collapse of the gas bubble in the high pressure region thus causing a sudden increase in the local pressure values. The minimum pressure values generated in squeeze film were not sufficient and did not fall below the saturation pressure of Mobil oil for vapor cavitation to occur.
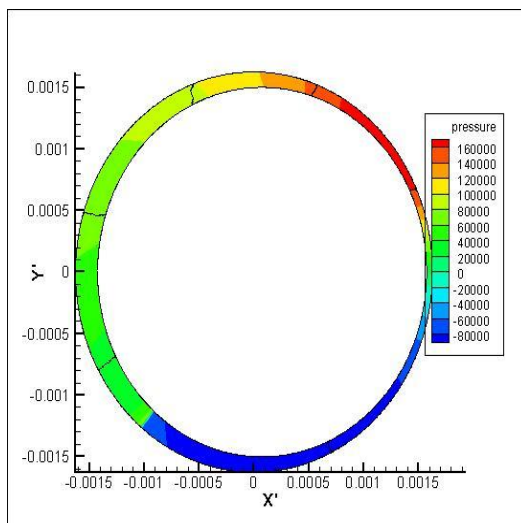

Figure 28: Pressure distribution for a section at mid land operating at 100Hz
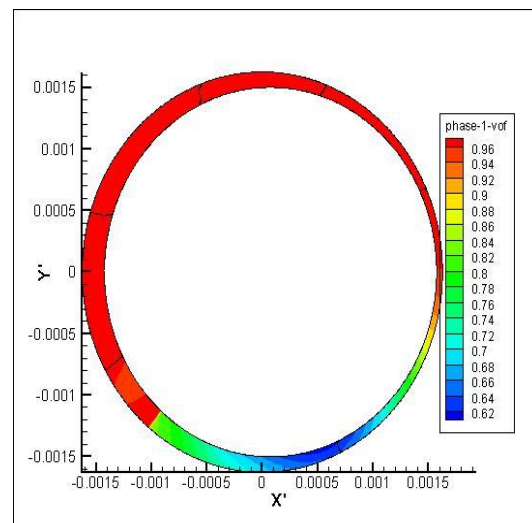
Figure 29: Liquid fraction distribution for a section at mid land operating at 100Hz
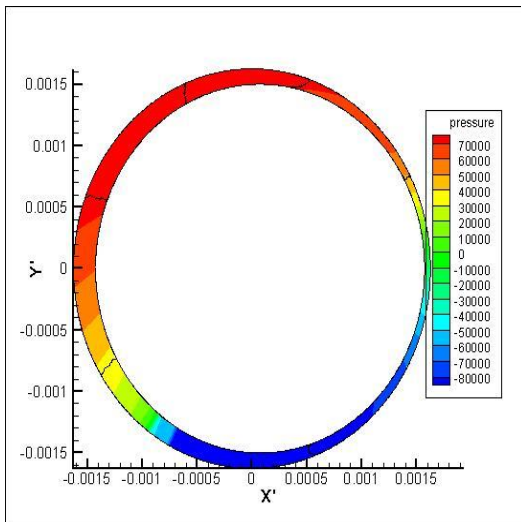
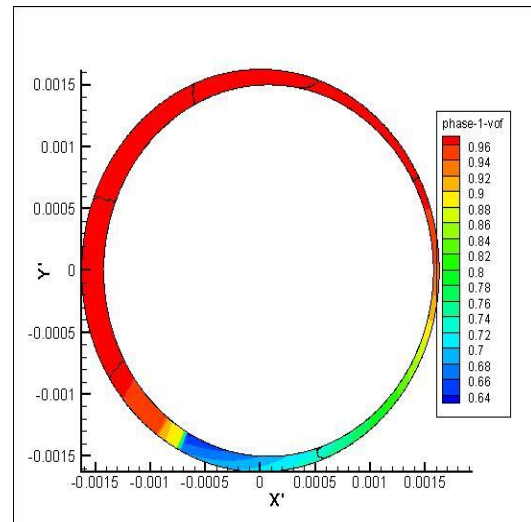**Figure 30: Pressure distribution for Section-1 operating at 100 Hz**

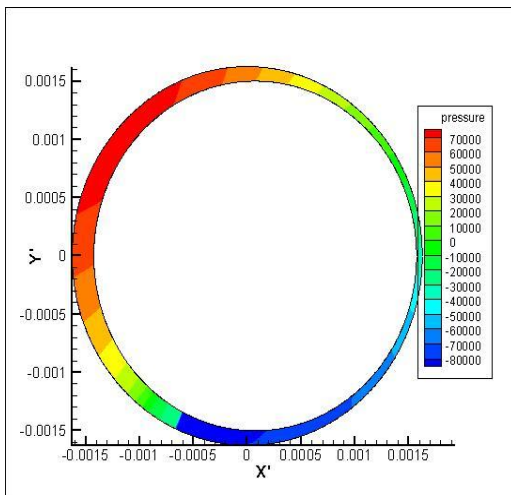**Figure 31: Liquid fraction for section-1 operating at 100Hz**

Figure 32: Pressure distribution for Section-5 operating at 100 Hz
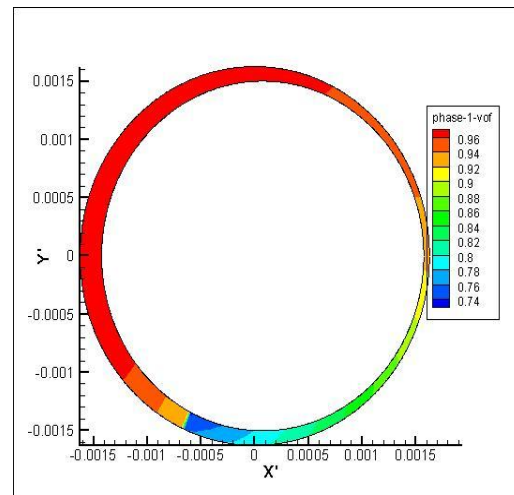

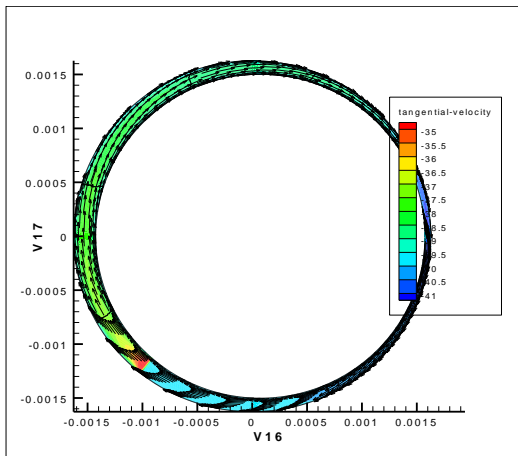**Figure 33: Liquid fraction for section-5 operating at 100Hz**

Figure 34: Tangential velocity at 100 Hz in moving reference frame
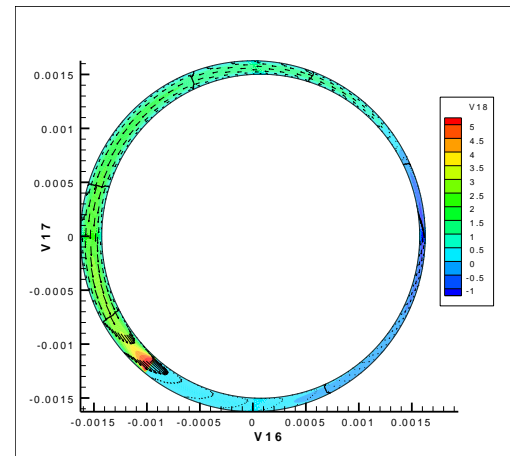
Figure 35: Tangential velocity at 100 Hz in stationary reference frame

The maximum, minimum pressure and volume fraction values are higher for 100 Hz case than 50 Hz case thus generating more forces. The spread of the liquid fraction for case at higher speed (100 Hz) is also wider. From Figures 28-29 34 and 35, it can be seen that there is a sudden increase in tangential velocity and liquid fraction value at -130°. Pressure also increases but not as rapidly as tangential velocity or liquid fraction. Increase in tangential velocity and liquid fraction occur slowly for 50 Hz case. The sudden increase in 100 Hz case can be explained due to sudden appearance and collapse of the air bubble. Density of the mixture decreases as the bubble is formed which increases the tangential velocity suddenly. Figures 30-33 represent pressure and vof distribution for sections-1and 5. For journal bearing operating at 100 Hz the maximum theoretical pressure is 1527200N/m^2 as compared to 160000N/m^2 for the squeeze film damper which is twice the 50 Hz case. It can be seen that difference in magnitude reduces for 100Hz case. As shown in Figures 36 and 37 the variation of pressure

distribution with axial length at maximum and minimum pressure locations for 100 Hz

also takes quadratic form just as in case of journal bearings.
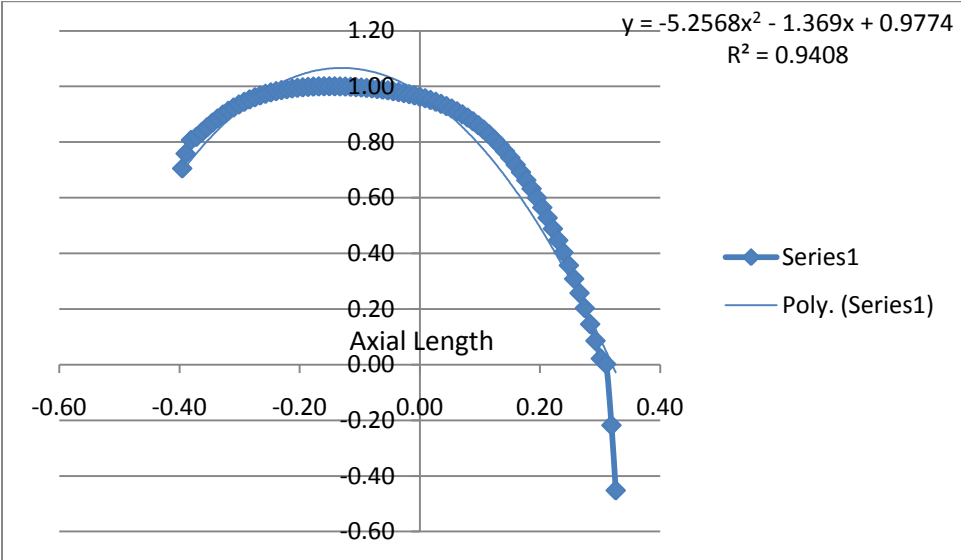
Figure 36: Pressure distribution along axial direction at minimum pressure location (100Hz)
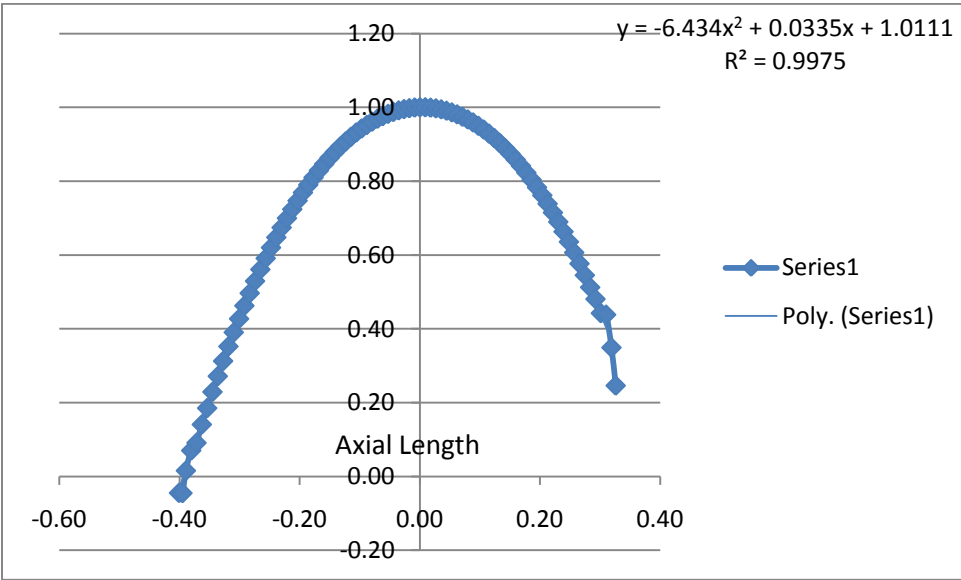
Figure 37: Pressure distribution along axial direction at maximum pressure location (100Hz)
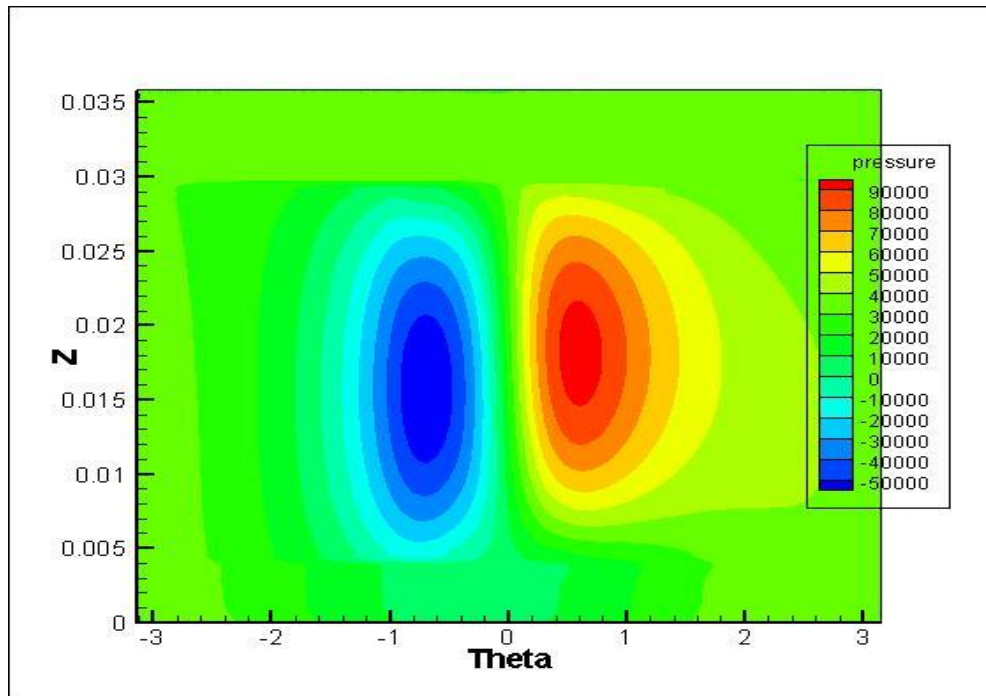
Figure 38: Pressure on rotor operating at 50 Hz
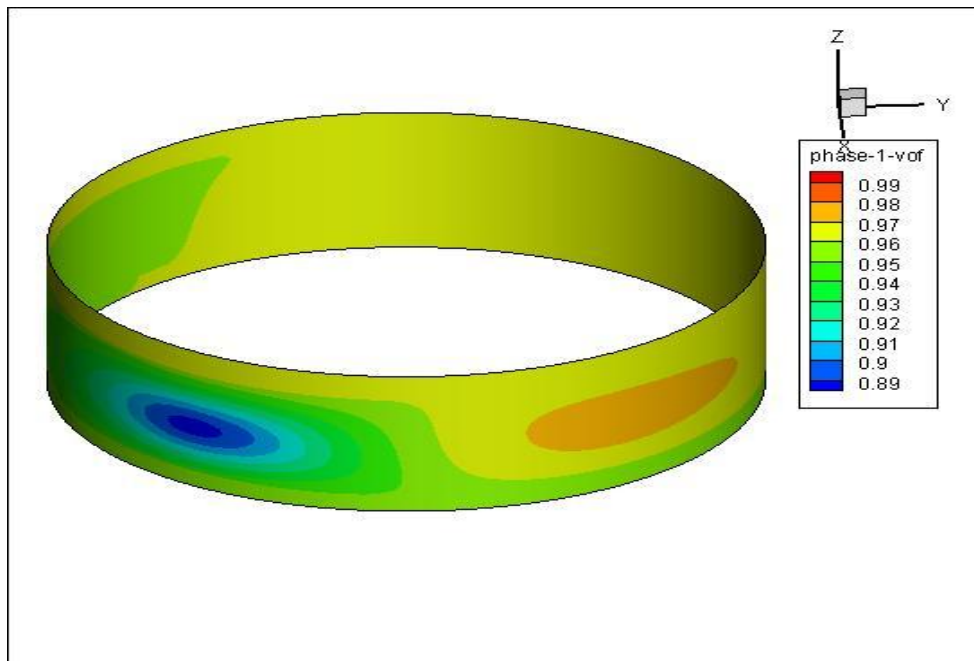
Figure 39: Liquid fraction on rotor operating at 50 Hz.
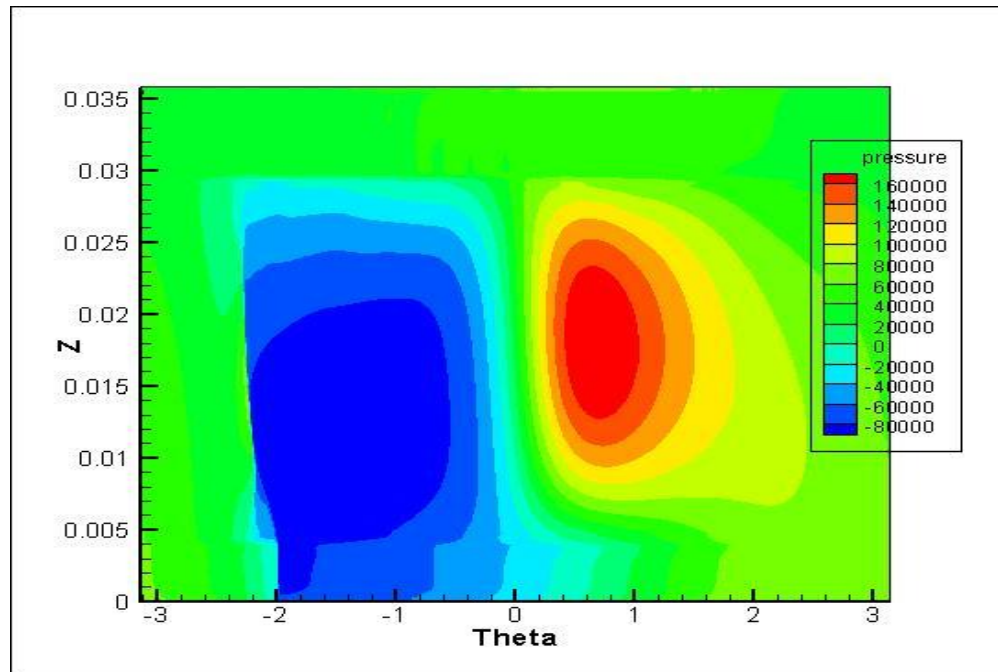
Figure 40: Pressure on rotor at 100 Hz
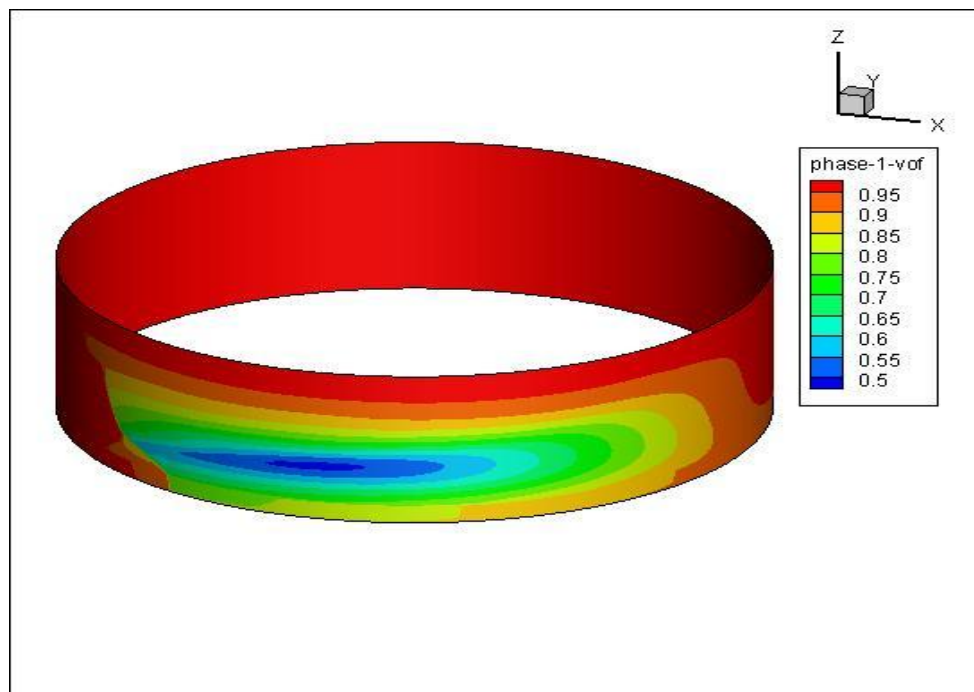
Figure 41: Liquid fraction on rotor at 100Hz
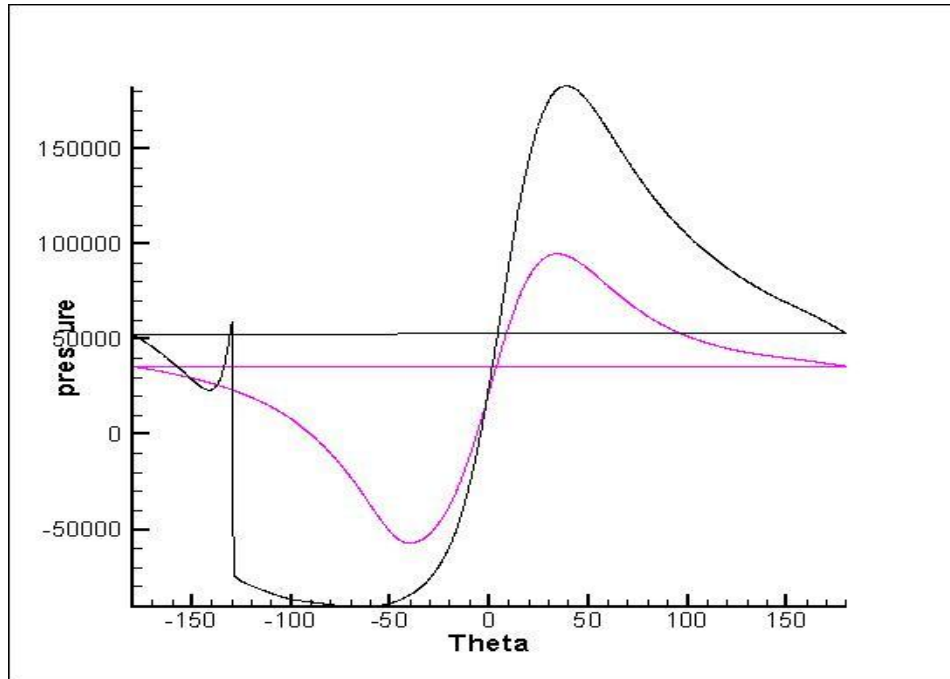
Figure 42: Comparison of pressures on rotor at 50 & 100Hz
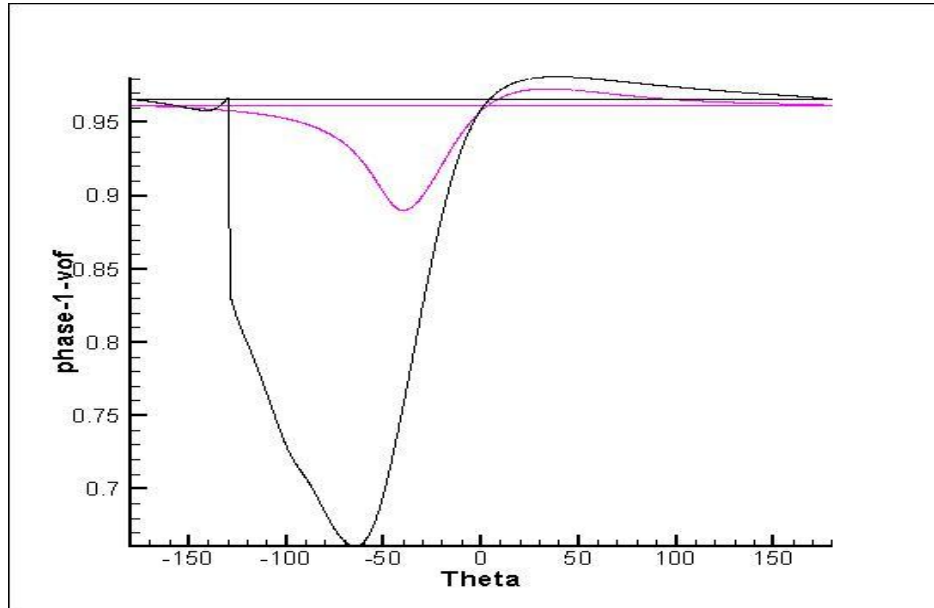
Figure 43: Comparison of liquid fraction on rotor at 50 & 100Hz
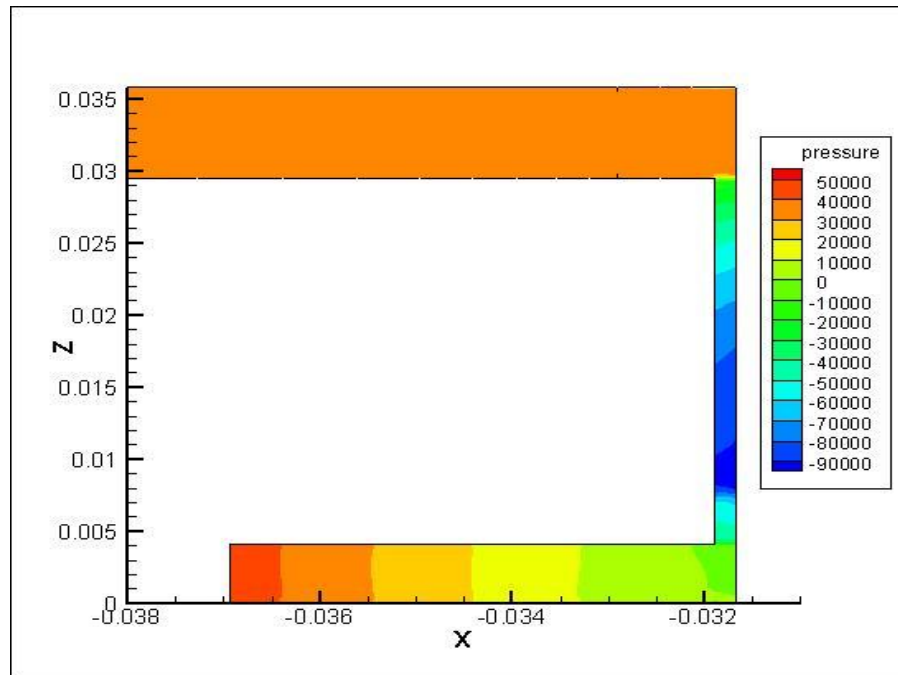
Figure 44: Pressure contour at axial section just before bubble collapse
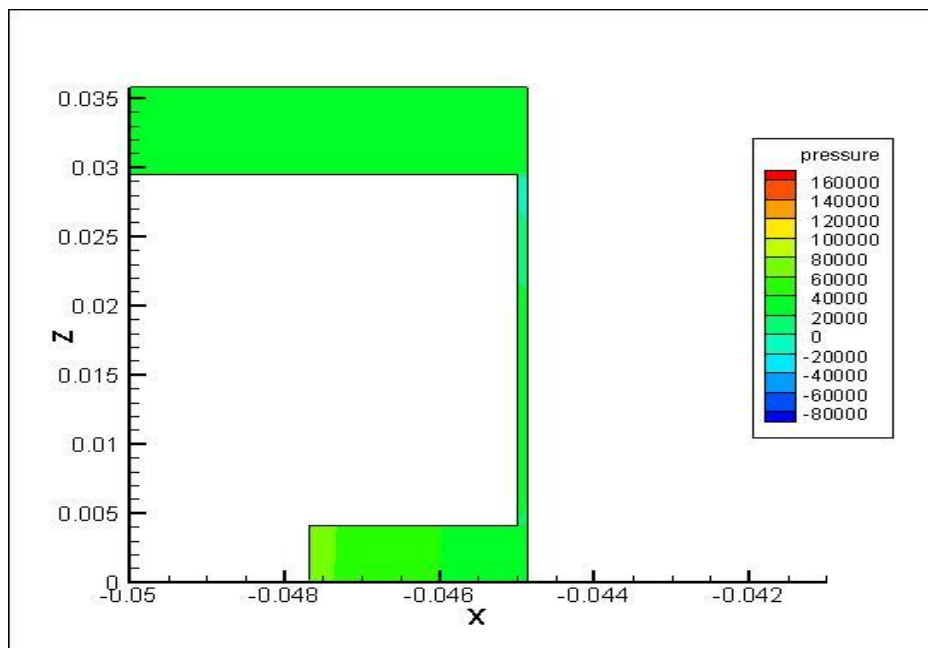
Figure 45: Pressure contour at axial section just after bubble collapse

Figures 38-41 represent pressure and vof contours for 50 and100 Hz cases. From Figure 42 it can be seen that the spread of minimum pressure for 50 Hz is from -20 degrees to -70 degrees while for 100 Hz case is from -20 degrees to -130 degrees indicating that as the speed increases the spread of minimum pressure becomes wider. The pressure curve for 100 Hz case, in low pressure region of its cycle, jumps suddenly from -70kpa to 50kpa due to cavitation occurring at low pressures. The cavitation occurring in low pressure region is due to sudden collapse of gas bubble. Therefore at higher orbiting speeds cavitation effects occur more quickly in the theta direction causing a very sudden and large pressure gradient. This moving pressure gradient over a small distance produces sudden stresses in the stator and rotor. Cyclic fatigues as well as cavitation erosion are introduced more quickly at higher speeds. Figure 43 shows the effect of cavitation as the speed is increased. An increase in liquid fraction (volume fraction of air) to almost three times the value of liquid fraction observed when operated at a speed of 50 Hz can be seen. Lower the speed the lesser the effect of cavitation.

The rotor progresses in positive theta direction. For SFD the fluid is pushed in front of the rotor (0°-180°) while there is a wake behind the rotor (-180°-0°) with the minimum clearance at 0°. The flow rate around the circumference is constant at the land center. Between theta 180° and 0° the clearance is decreasing which implies that the pressure is decreasing according to Bernoulli's equation. However in this case the fluid is pushed around by the rotor and is accelerated by the push accompanied by an increase in pressure from 180° to 30°. Thus the largest pressure is attained at 30° for both the

speeds. The pressure then decreases from 30° to 0° as the fluid attains the speed necessary to accommodate the rotor's motion.

Behind the rotor the channel increases in size from theta 0° to 180° and a wake is generated. This causes pressure to drop and gas to expand even more as the pressure decreases. This is followed by a pressure increase and volume fraction decrease as theta approaches -180°. The location of the minimum pressure and its magnitude vary with speed, at 50Hz the minimum pressure of -60 kPa and occurs at theta -40° and at 100Hz the minimum pressure of -90 kPa occurs at theta -70°. The shape of the curve is similar to Somerfield journal bearing but the locations of maximum pressure and magnitude different. At 100 Hz, the wake region is very different from the 50Hz case. The vof of 50Hz case never went below 90% and the flow was smooth and continuous. The vof at 100 Hz decreased to 66% at theta -65° and the pressure remained very low at -90,000 Pa from -30° to -120°. Suddenly the vof begins to rise rapidly with a sharp jump at -130°; there is a jump in pressure as well. The sharp jump indicates a collapse of bubbles in the wake and this sudden collapse of the bubbles results in large jump in V_t as liquid rushes in to occupy the space of the bubbles. The large V_t thus generated causes an overshoot in pressures as liquid velocity suddenly decreases in magnitude when the bubble volume is filled with liquid. The pressure and vof spike then dissipates as theta goes from -130° to -140°. From theta -140° to -180° the pressure and vof follows the general smooth trend as seen in 50Hz case. Figure 44-45 show pressure contours at axial sections just before and after bubble collapse. From the figures it can be seen that because of very low pressures bubbles are formed and as they see high pressures they collapse.

6.4 Effect of Central Groove

Figure 46: Liquid fraction distribution on rotor with central groove of 0.5 X 0.5 operating at 50Hz.
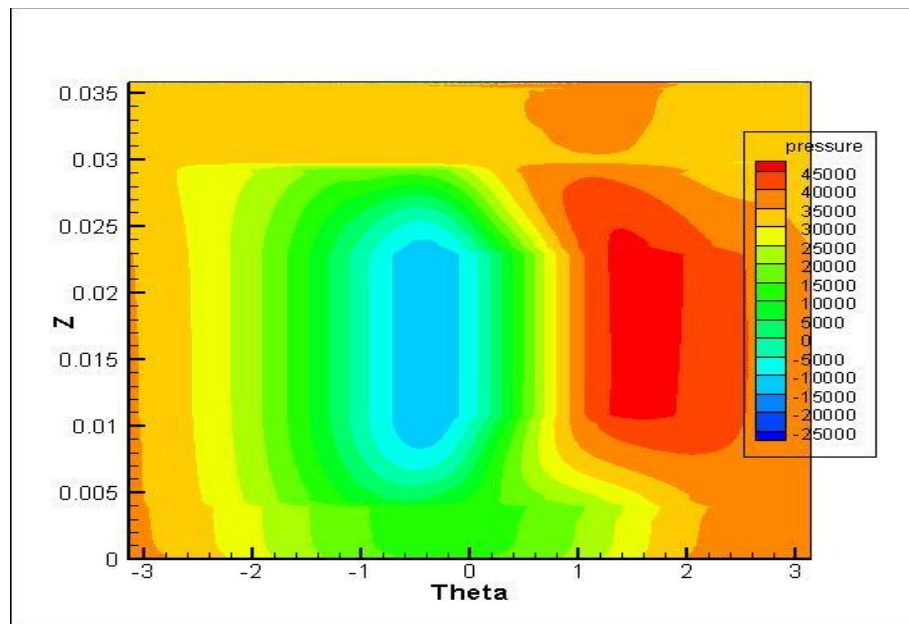
Figure 47: Pressure distribution on rotor with central groove of 0.5 X 0.5 operating at 50Hz.
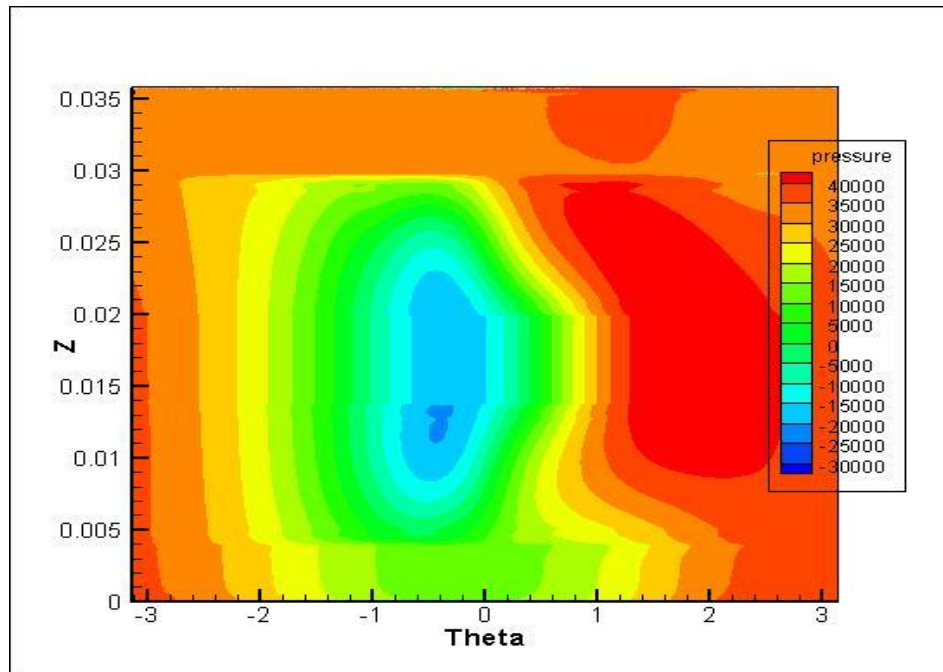
Figure 48: Pressure distribution on rotor with central groove of 1 X 0.25 operating at 50Hz
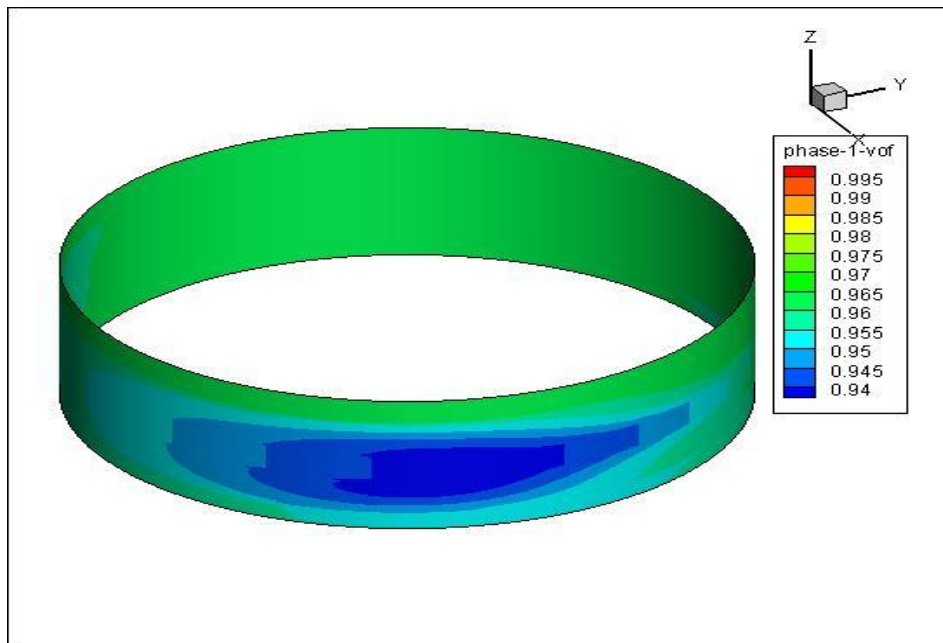
Figure 49: Liquid fraction distribution on rotor with central groove of 1 X 0.25 operating at 50 Hz
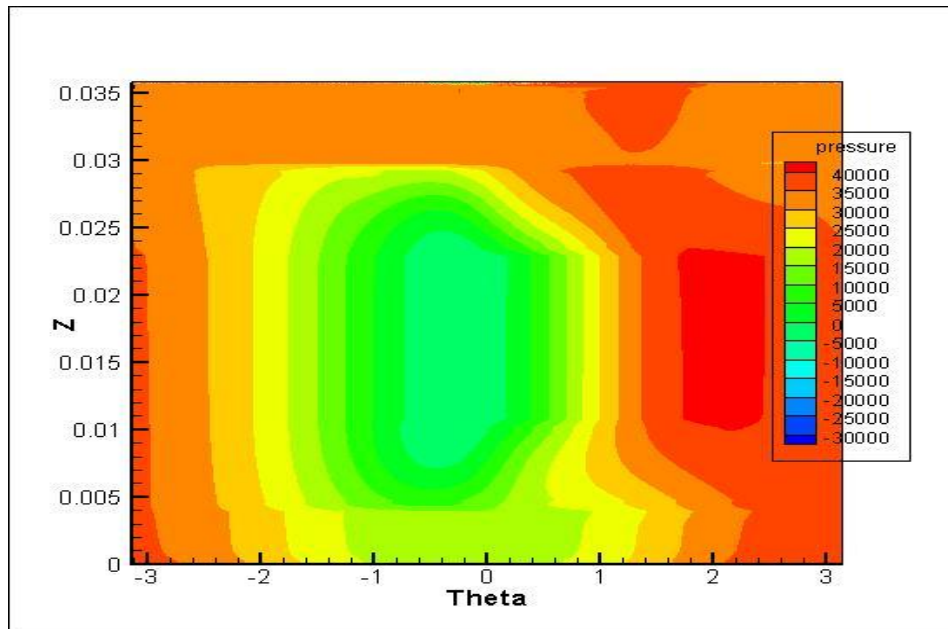
Figure 50: Pressure distribution on rotor with central groove of 1 X 0.5 operating at 50Hz
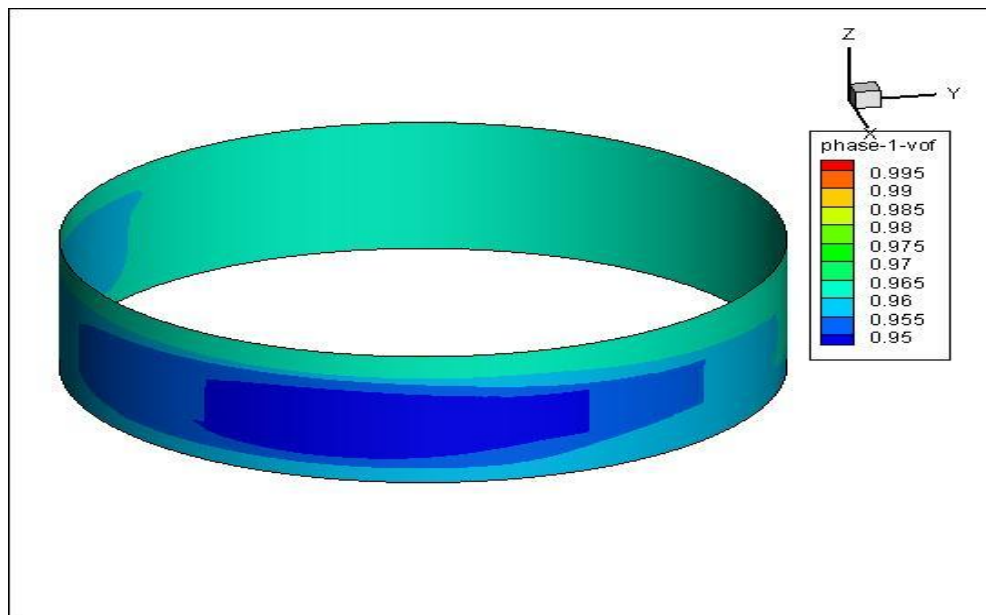
Figure 51: Liquid fraction distribution on rotor with central groove of 1 X 0.5 operating at 50Hz
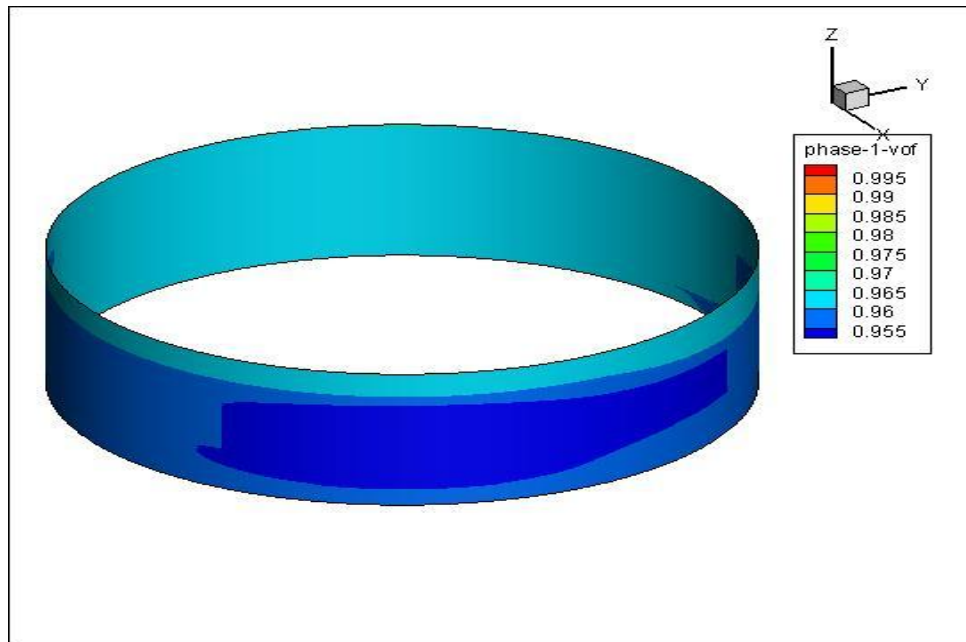
Figure 52: Liquid Fraction distribution on rotor with central groove of 2 X 0.5 operating at 50Hz
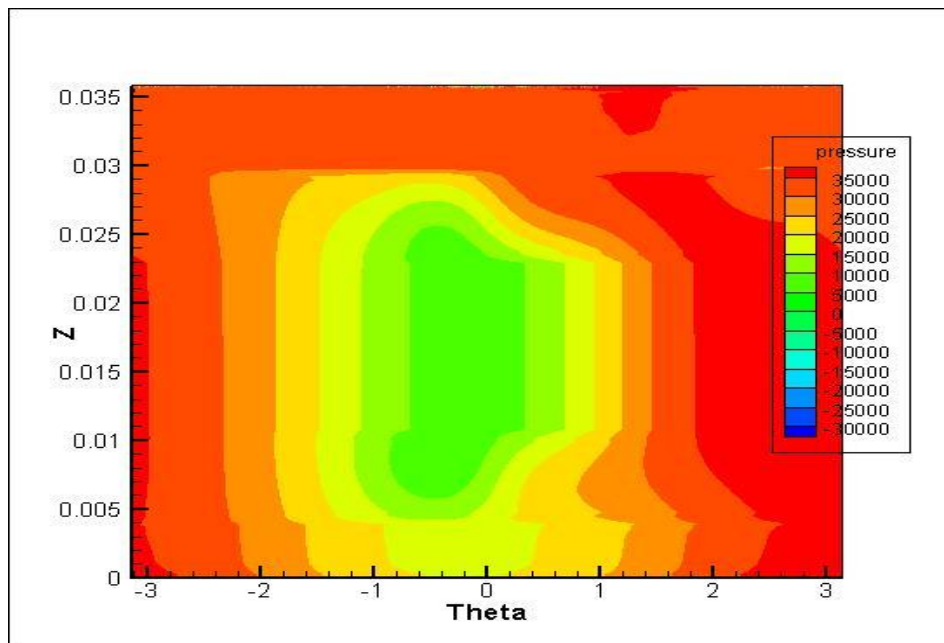
Figure 53: Pressure distribution on rotor with central groove of 2 X 0.5 operating at 50Hz

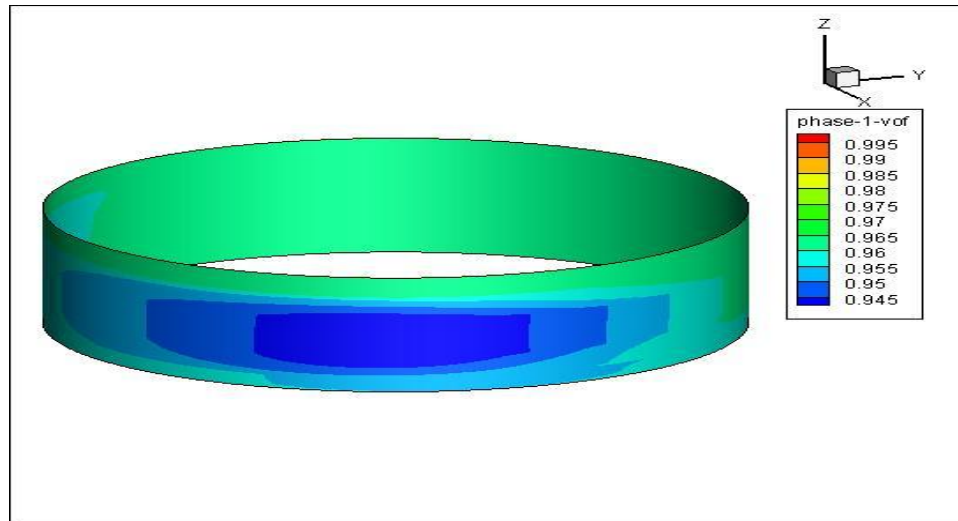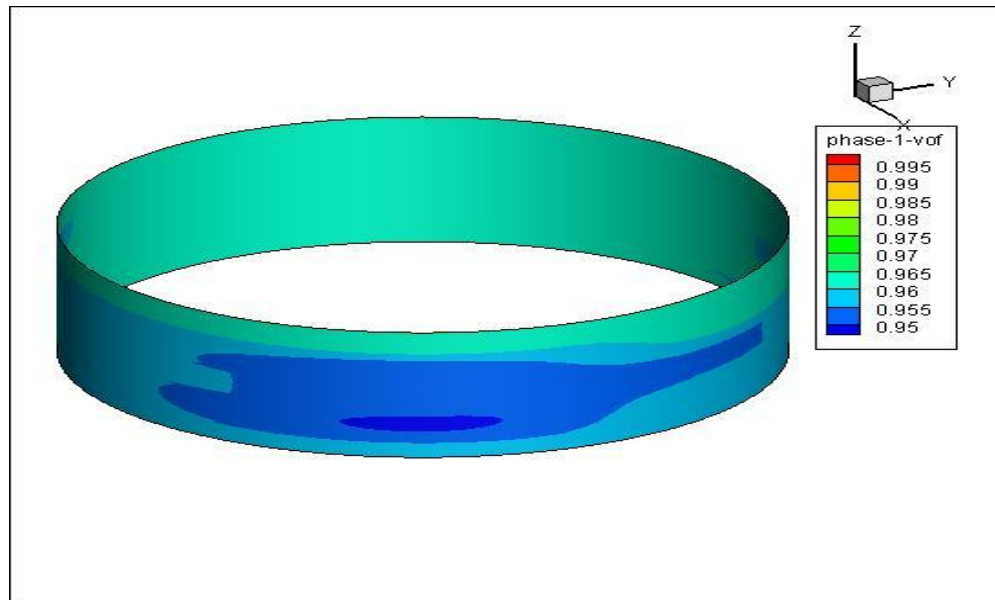**Figure 54: Liquid fraction distribution on rotor with central groove of 4 X 0.25 operating at 50Hz**
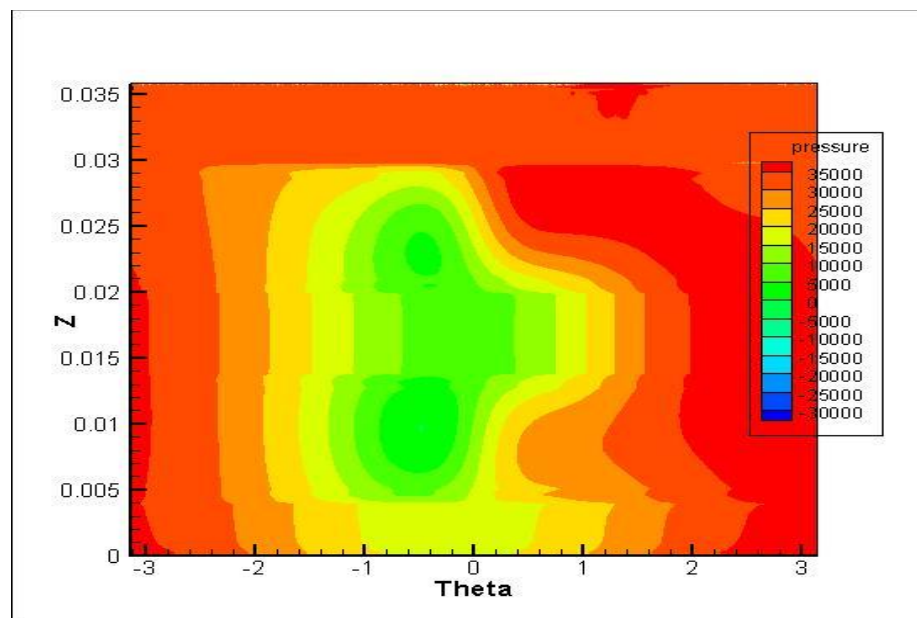
Figure 55: Pressure distribution on rotor with central groove of 4 X 0.25 operating at 50Hz
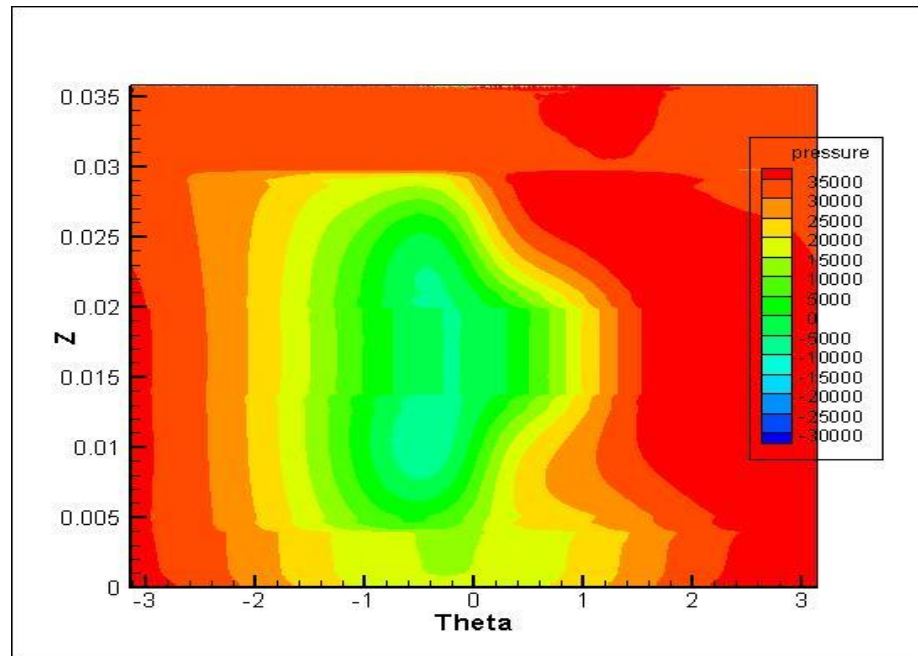
Figure 56: Pressure distribution on rotor with central groove of 2 X 0.25 operating at 50Hz
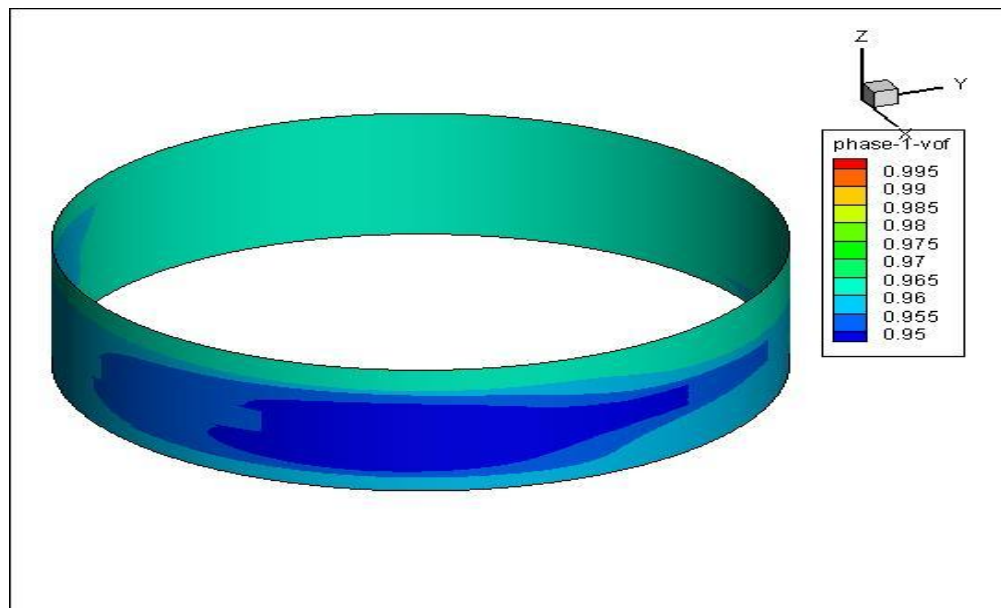
Figure 57: Liquid fraction distribution on rotor with central groove of 2 X 0.25 operating at 50Hz
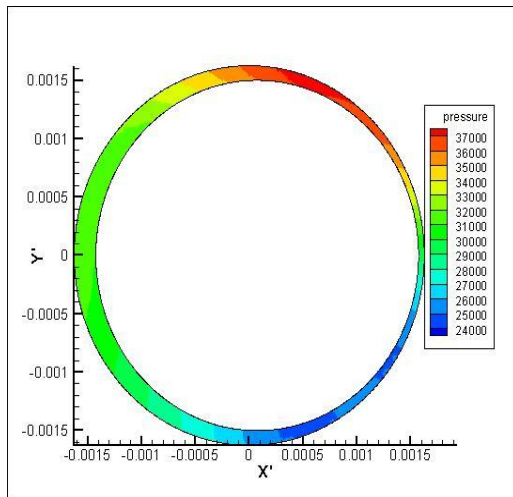
Figure 58: Pressure distribution Sec-1 with 0.5 X 0.5 groove operating at 50Hz
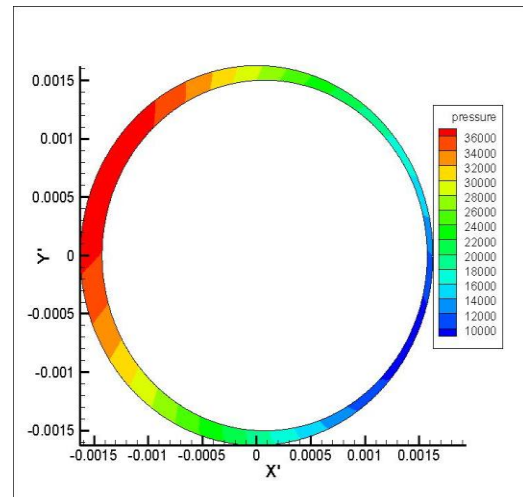
Figure 59: Pressure distribution at sec-5 with 0.5 X 0.5 groove operating at 50Hz
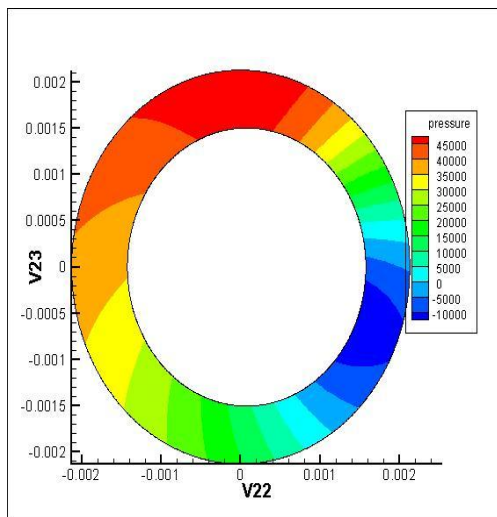
Figure 60: Pressure contours at mid-section of SFD with central groove of 0.5 x 0.5 operating at 50 Hz.
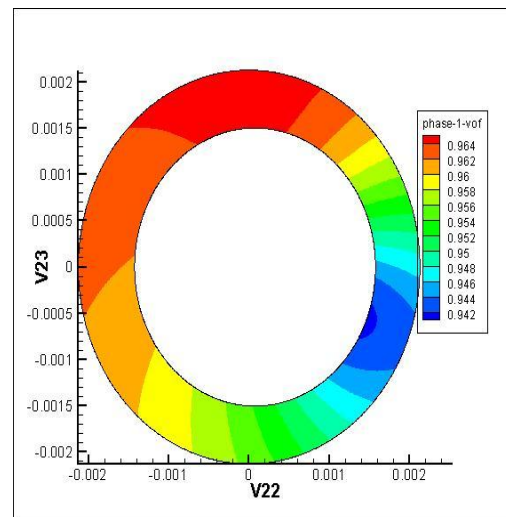
Figure 61: Liquid fraction at contours at mid-section of SFD with central groove of 0.5 x 0.5 operating at 50 Hz.

Table 2: Maximum and minimum pressure for different groove sizes

Groove Size	Groove Area(m^2)	Pmax(kpa)	Pmin(kpa)
0.5-0.5	6.35	45	-15
1-0.25	6.35	40	-25
1-0.5	12.7	40	-10
2-0.25	12.7	35	-10
2-0.5	25.4	35	0
4-0.25	25.4	35	0

Figures 46 to 57 show that equal volumes of the central groove have equal effect on Liquid fraction and pressures developed in the squeeze film land, with all of them reducing the amount of vapor formed. The highest pressure and lowest pressure developed in the squeeze film land with a central groove are half of that developed in a smooth SFD, with pressure values decreasing slightly as the groove size increases for the range of the dimensions tested. The pressure contours clearly show the area occupied by the groove. From Table 2 it can be seen that for the groove with smallest cross sectional area of 6.35 mm^2 the maximum and minimum pressure varies slightly with the dimensions of the groove. As the area of cross section increase the variation of pressure with dimensions of the groove decreases. The maximum pressure distribution remains relatively constant with increasing cross sectional area. Pressure distribution varies along the axial length of the SFD as the cross sectional area decreases. Minimum pressure shows more axial dependence than maximum pressure for all cases. The liquid fraction value tends to minimize at 94% for all the cases with its lowest value occurring at the groove. Figures 58 and 59 represent pressure profiles at section 1 and 5 of the squeeze

film damper which are immediately after the inlet (6.35mm from top) and before the discharge groove (4.1mm from bottom) respectively. Figures 60 and 61 represent the pressure and liquid fraction contours at mid land section of the central groove of dimension 0.5 X 0.5 in the moving reference frame. These figures show that pressure and liquid fraction have a slight radial dependence at section-1 while the radial dependence of pressure and liquid fraction is more significant at the mid land due to the presence of the central groove. Figure 62 show pressure distribution for the same configuration in three dimensional view.
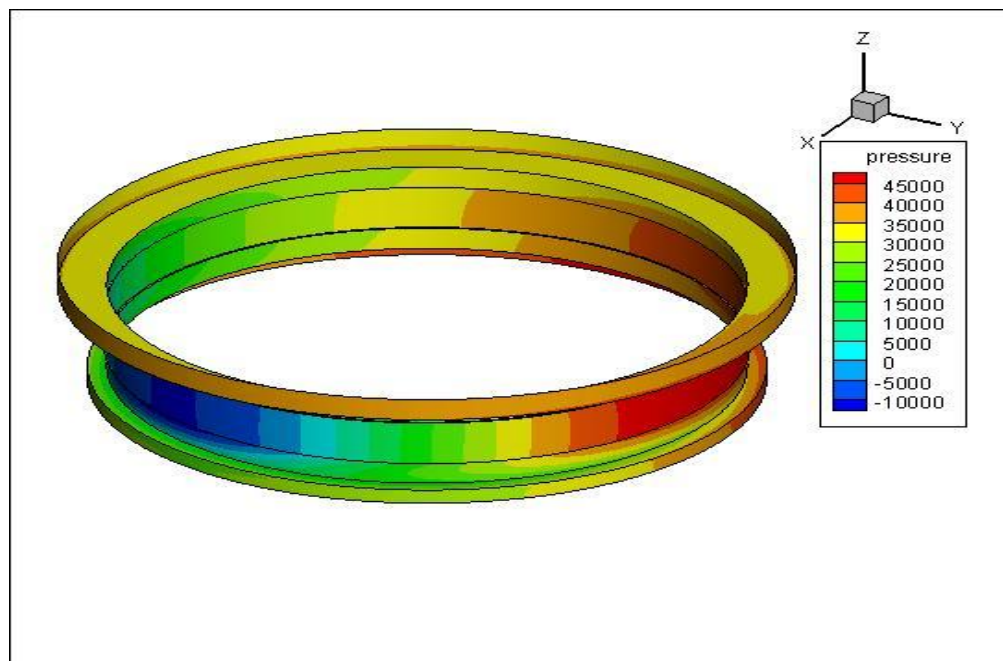
Figure 62: Pressure distribution on stator with central groove of dimension of depth 0.5mm and length 12.7mm
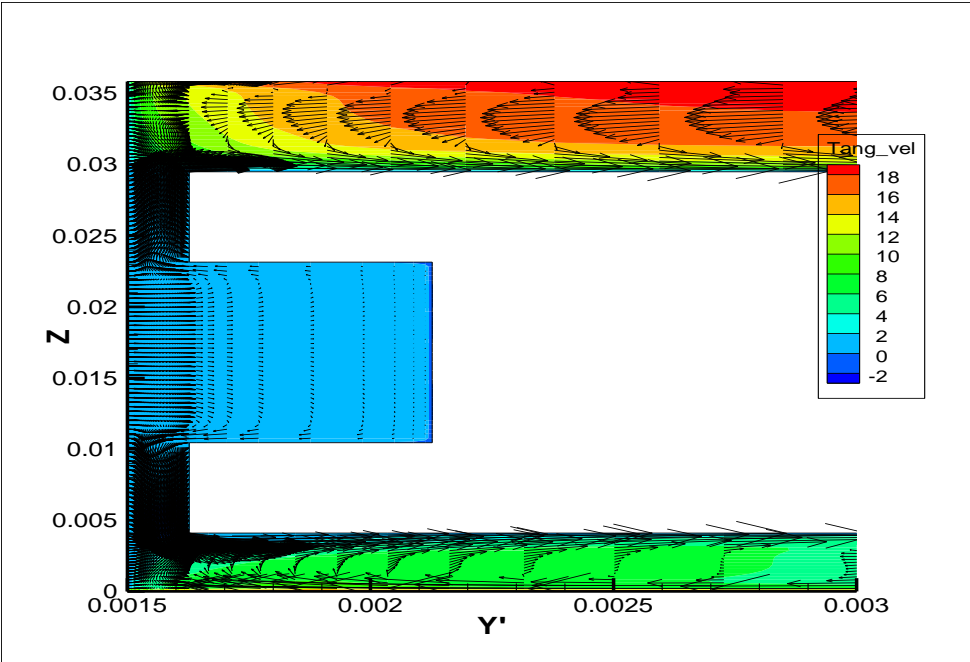
Figure 63: Vectors of axial velocity on a section at 90 degrees
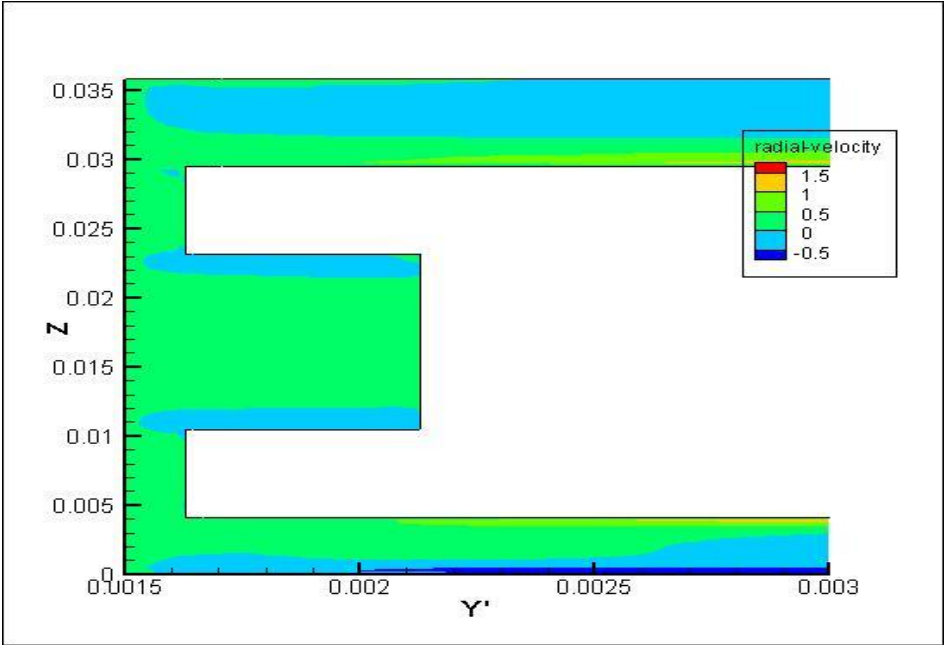
Figure 64: Radial velocity contours for a section at 90 degrees
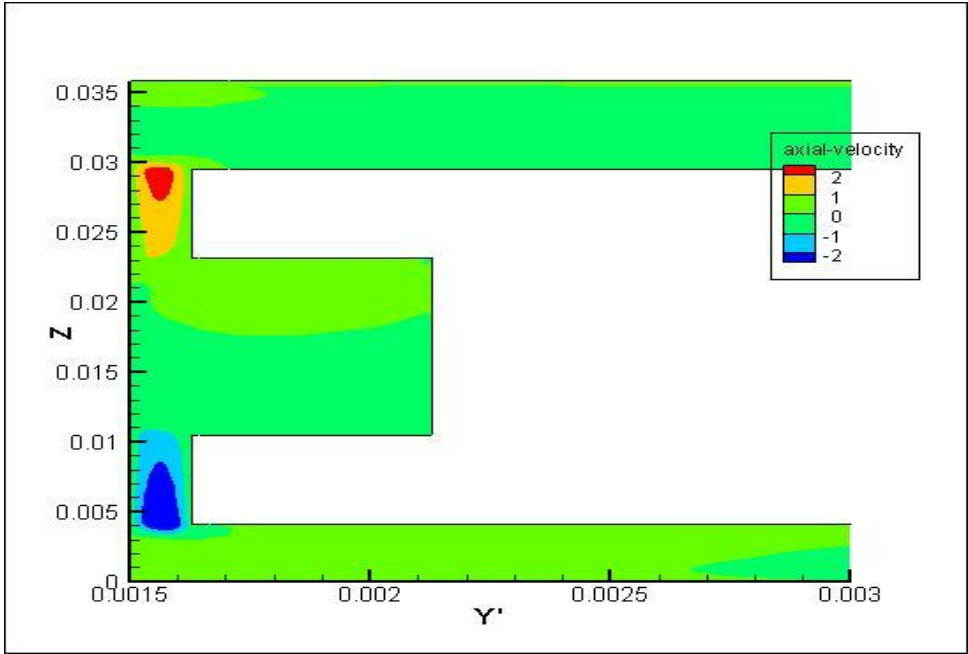
Figure 65: Axial velocity contours for a section at 90 degrees
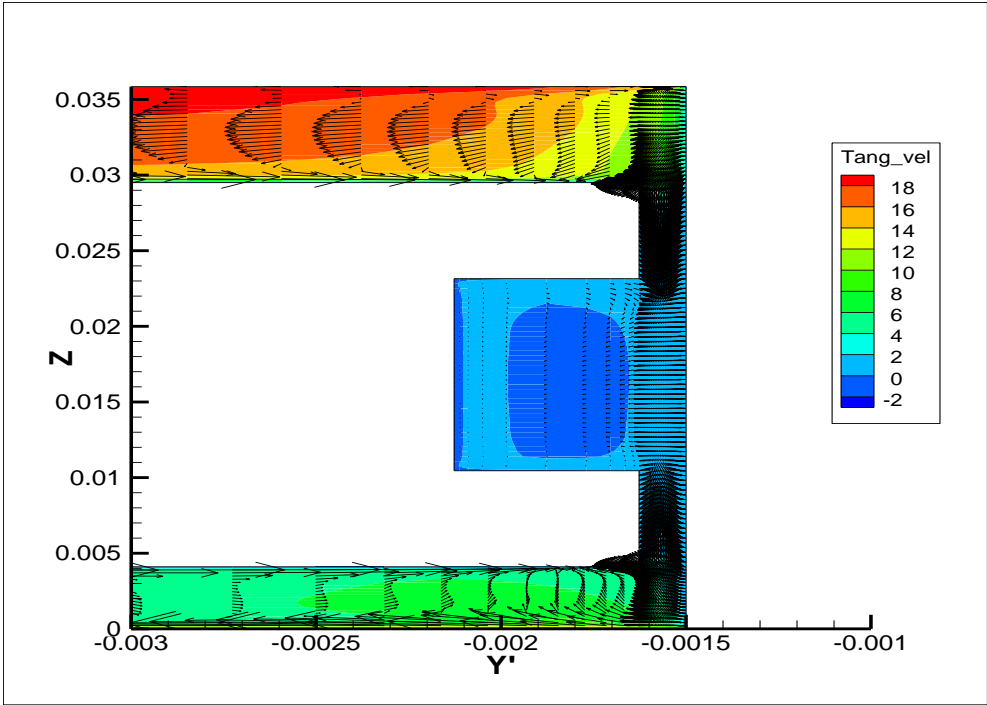
Figure 66: Vectors of axial velocity on a section at 270 degrees
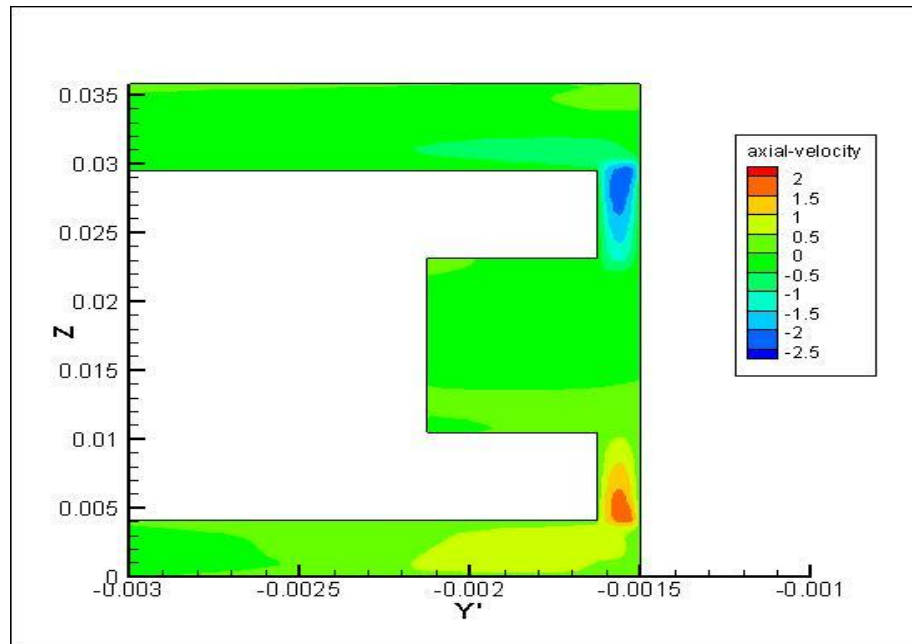
Figure 67: Axial velocity contours for section at 270 degrees
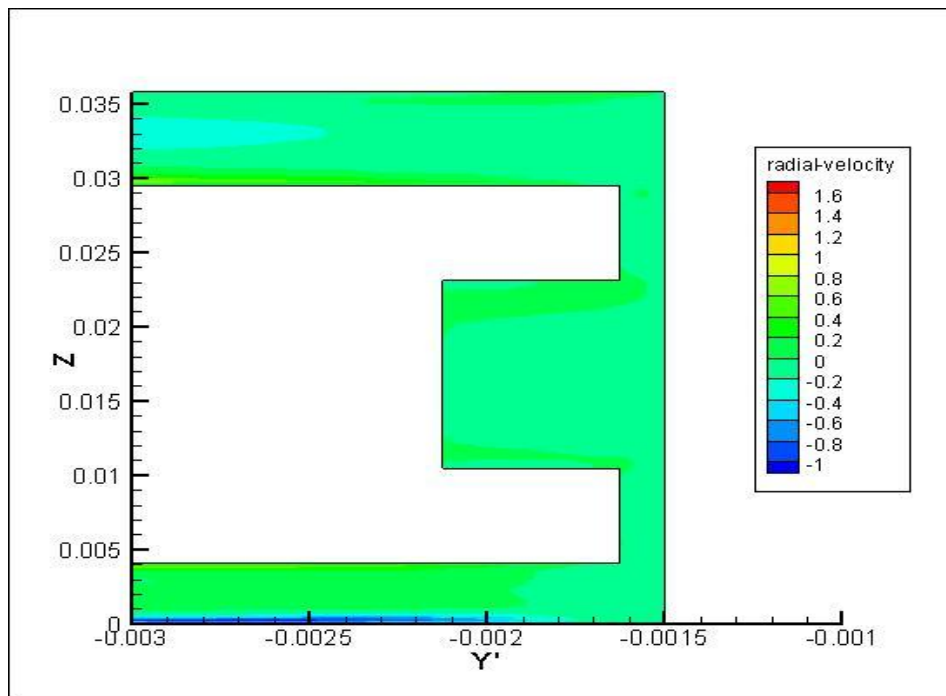
Figure 68: Radial velocity contours for a section at 270 degrees
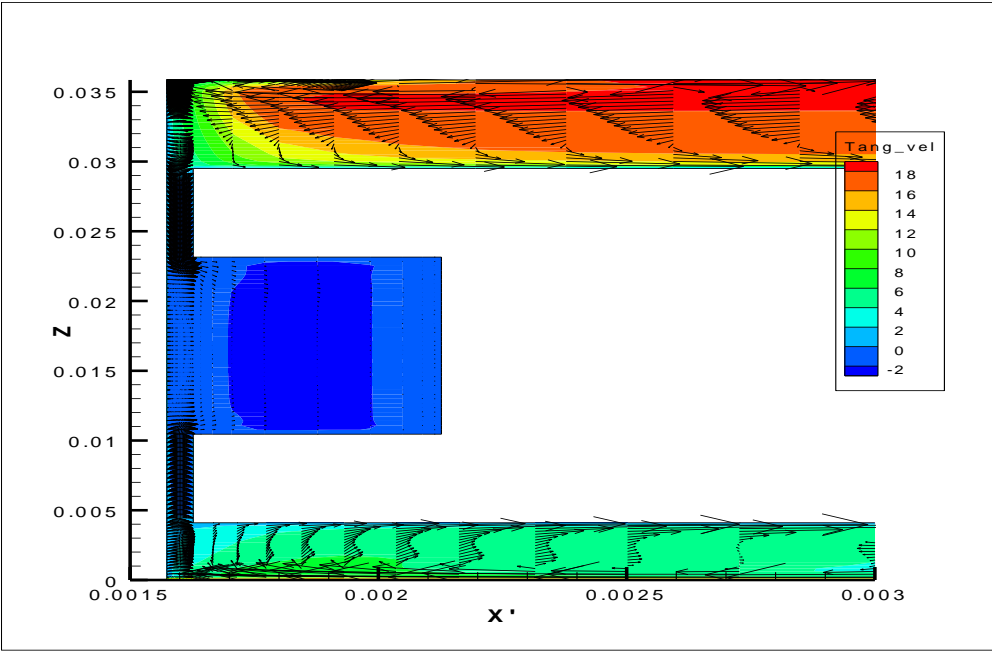
Figure 69: Vectors of axial velocity on a section at 0 degrees
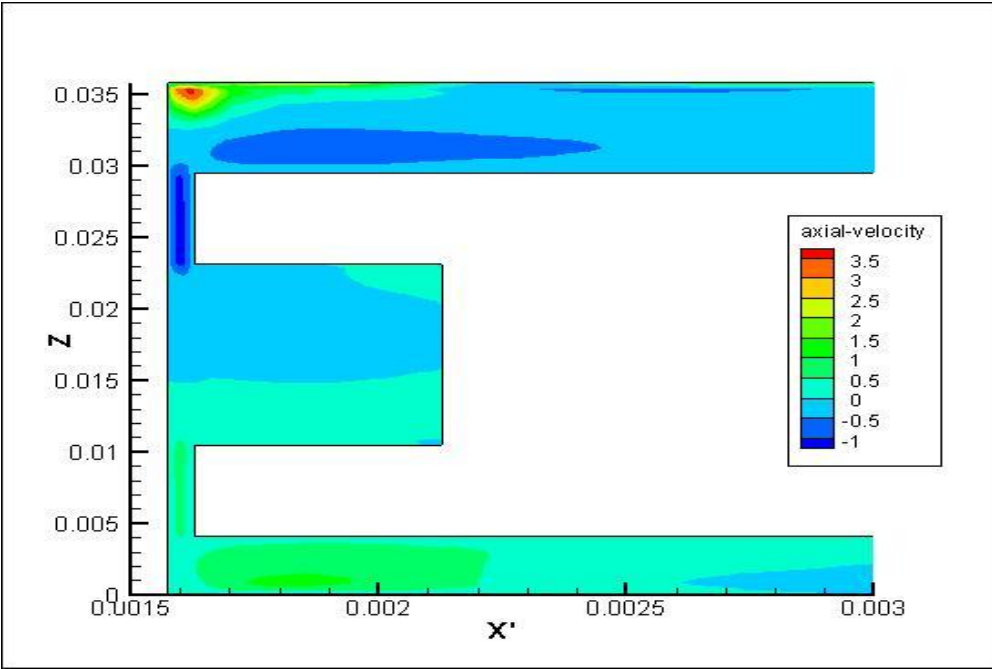
Figure 70: Axial velocity contours on a section at 0 degrees
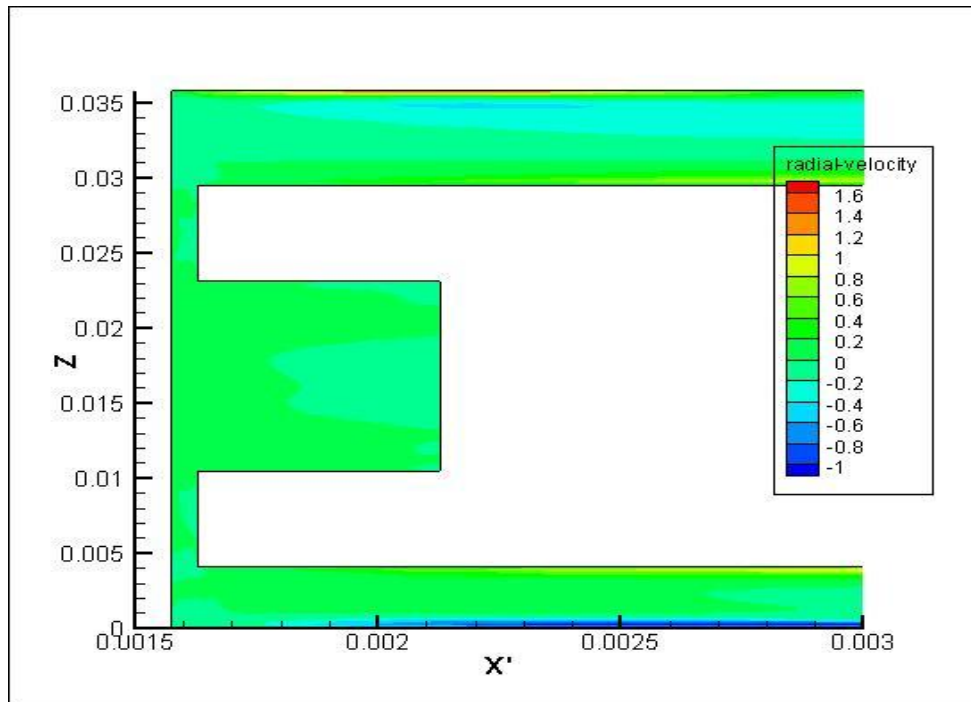
Figure 71: Radial velocity contours on a section at 0 degrees
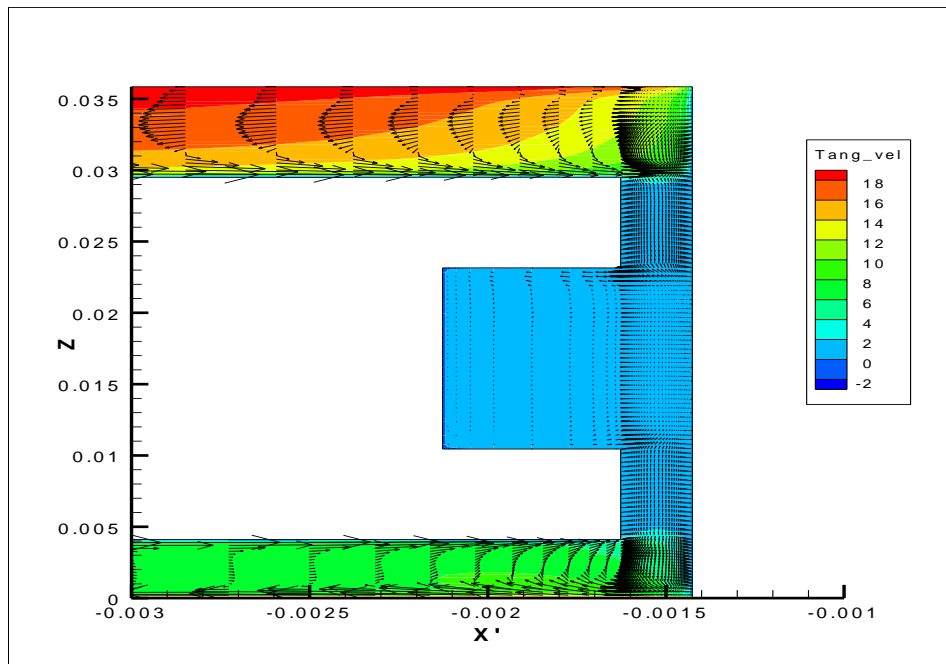
Figure 72: Vectors of axial velocity on a section at 180 degrees
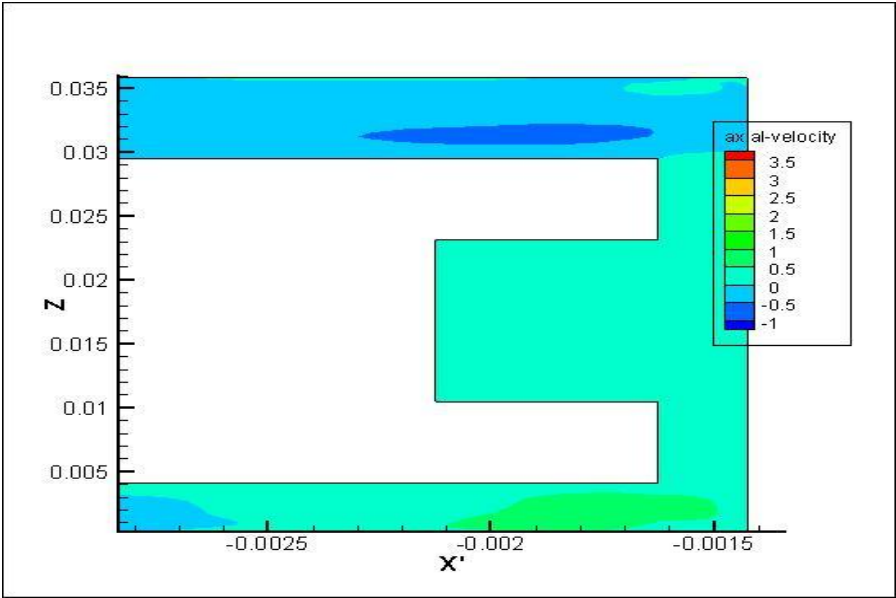
Figure 73: Axial velocity contours for a section at 180 degrees
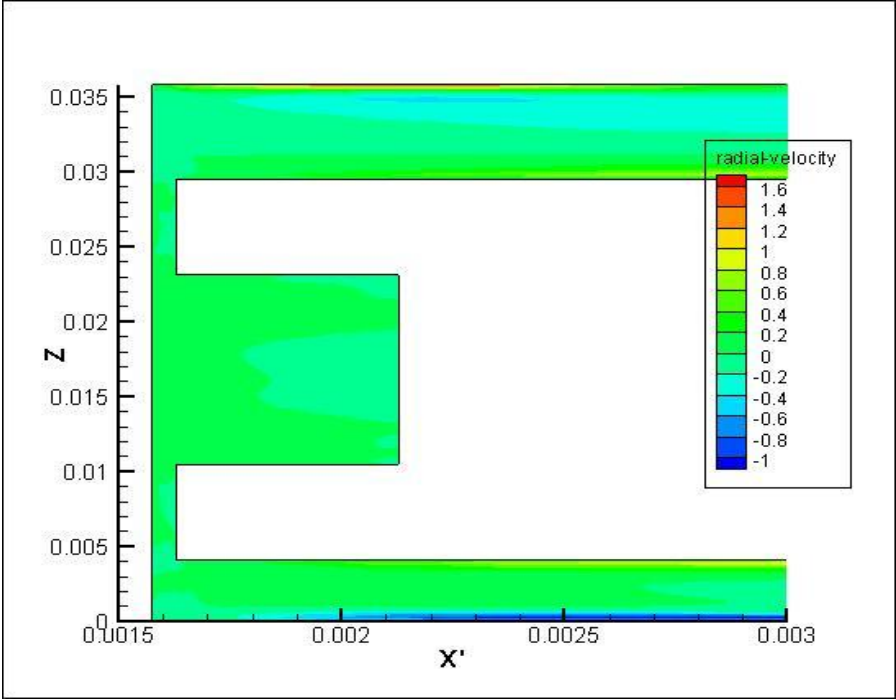
Figure 74: Radial velocity contours for a section at 180 degrees

Figures 63 to 74 present the tangential velocity contours with axial velocity vectors, radial, and axial velocity contours at different angular sections of 0°, 90°, 180°, 270°. It can be seen that in the section at 0° (minimum clearance) flow traverses the SFD land towards the central groove, at 90° flow is moving away from the central groove. In the section at 180°, axial flow is moving upwards across both the lands from discharge groove to the inlet groove with recirculation in the central groove. At 270° flow is again towards the central groove across both the lands. Comparing pressure contours from the previous figures it can seen that the flow is moving from low pressure regions to high pressure regions and thereby flow is being pushed into the central groove. Therefore, instead of developing pressure in the lands above and below the central groove the pressure increases in the central groove region. The extra volume of the central grooves reduces the magnitude of the pressures developed in that region and thus the magnitude of forces generated in the SFD.
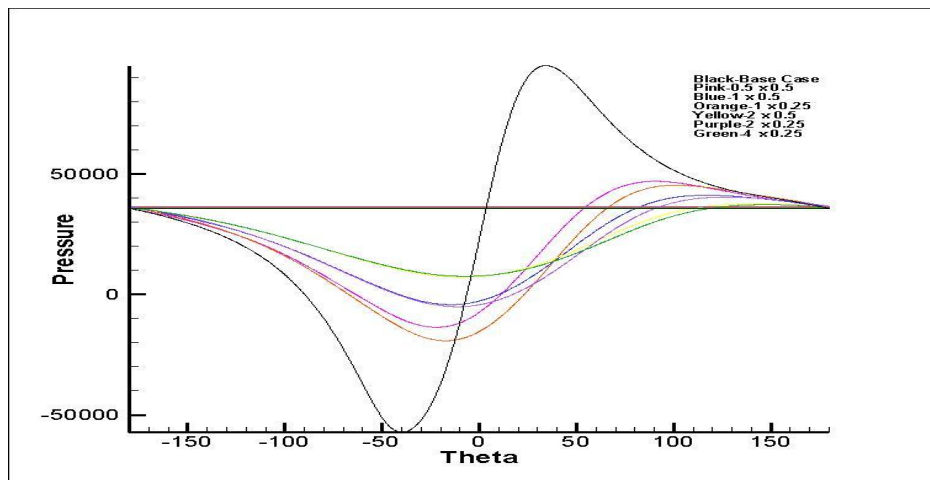
Figure 75: Comparison of pressure distribution on rotor for different central groove depths against smooth SFD operating at 50Hz

Hence the addition of the central groove becomes an effective method for reducing the pressures generated in the squeeze film land. From Figure 75, which is comparison graph for different configurations of SFD, it can be seen that when a central groove is added on the squeeze film land, the lowest and highest pressures generated at the mid land are reduced. There is a slight change in the position of occurrence of highest and lowest pressures depending upon the size of the central groove. But in general, it can be seen that for the range of configurations simulated, the pressures generated are reduced to half the values generated when run without any central groove in it. It can also be seen that the lines of equal volumes overlap on each other i.e. the amount of reduction in pressure values depends on the volume of the groove, not the length and the depth of the groove.

6.5 Effect of Central Groove at 100Hz

Figures 76 and 77 present the pressure and vof data for the SFD configuration operated at 100 Hz, which has central groove dimensions of 0.5mm x 0.5inch. The pressures developed and vapor generated in the squeeze film land are reduced by 30% compared to that generated in the smooth SFD run at the same speed. The spread of the low pressure and high pressure region remains same in magnitude and position. Rigidity of the SFD when run at 100Hz is reduced by adding the central groove on the squeeze film land and effect of cavitation is also reduced. The contours are similar to the no land except the pressures remain relatively constant across the groove. The sudden collapse of the bubble is still present and is shown by sudden change in both pressure and vof

63

values. The length along the axis that is subjected to maximum pressure is more for the grooved SFD.
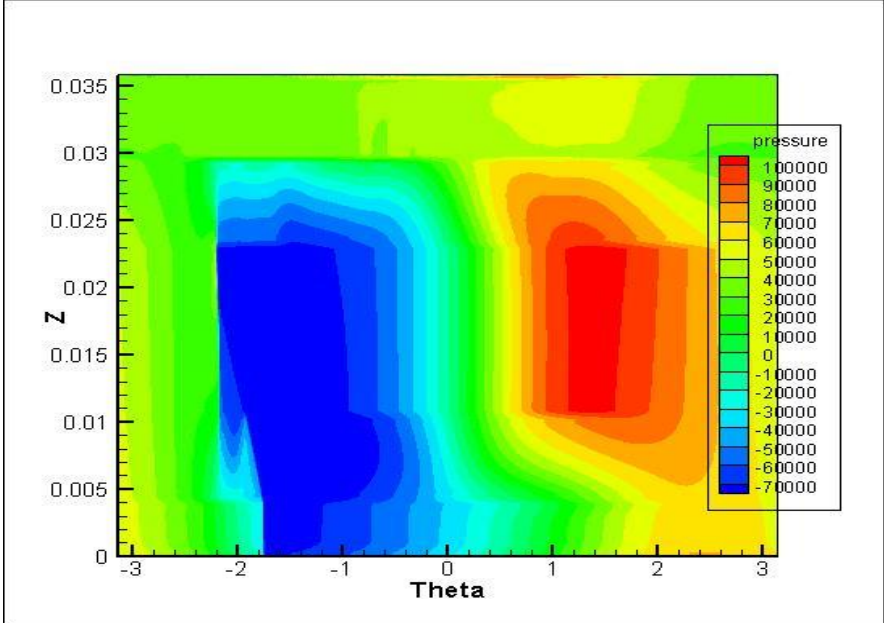
Figure 76: Pressure distribution on rotor with central groove of 0.5 X 0.5 operating at 100Hz
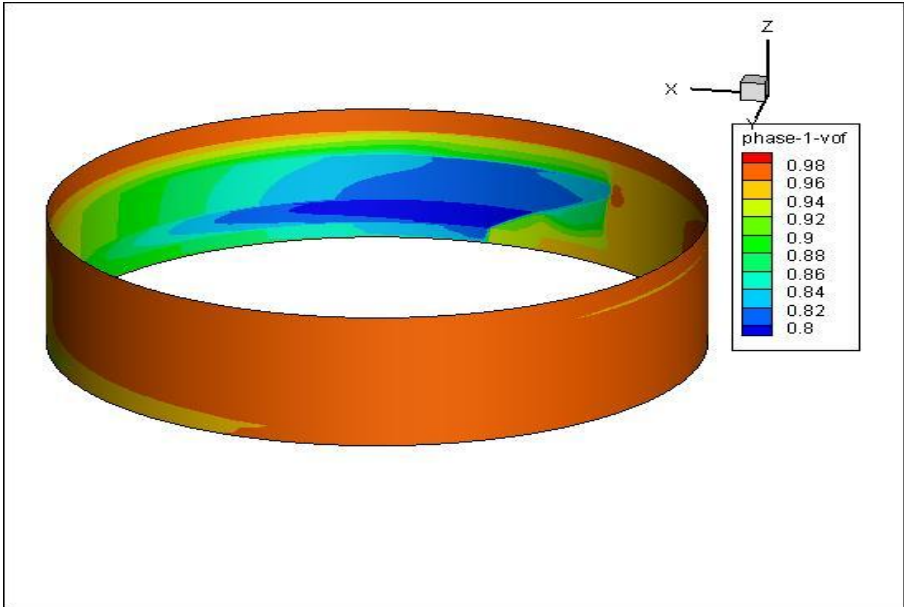
Figure 77: Liquid fraction distribution on rotor with central groove of 0.5 X 0.5 operating at 100Hz

Table 3: Comparison of forces generated for different groove configurations of SFD

Frequency(HZ)	Groove Depth(mm)	Groove Length(inch)/F_x	Cross sectional Area(mm^2)/F_y	Resultant
50	1	0.5	12.7	
pressure forces		-85.33	55.04	
Viscous forces		0.15	-0.16	
Total Force		-85.18	55.03	**101.41**
Angle				**147.2104**
50	2	0.25	12.7	
pressure forces		-83.26	57.6	
Viscous forces		0.19	-0.14	
Total Force		-83.07	57.46	**101.01**
Angle				**145.4019**
50	0.5	0.5	6.35	
pressure forces		-89.5	85.14	
Viscous forces		0.14	-0.22	
Total Force		-89.36	84.92	**123.27**
Angle				**136.5286**
50	1	0.25	6.35	
pressure forces		-98.41	83.9	
Viscous forces		0.18	-0.19	
Total Force		-98.23	83.71	**129.06**
Angle				**139.6337**
50	2	0.5	25.4	
pressure forces		-65.9	31.9	
Viscous forces		0.14	-0.11	
Total Force		-65.76	31.79	**73.04**
Angle				**154.2779**
50	4	0.25	25.4	
pressure forces		-62.15	39.6	
Viscous forces		0.13	-0.11	
Total Force		-62.02	39.49	**73.53**
Angle				**147.5887**
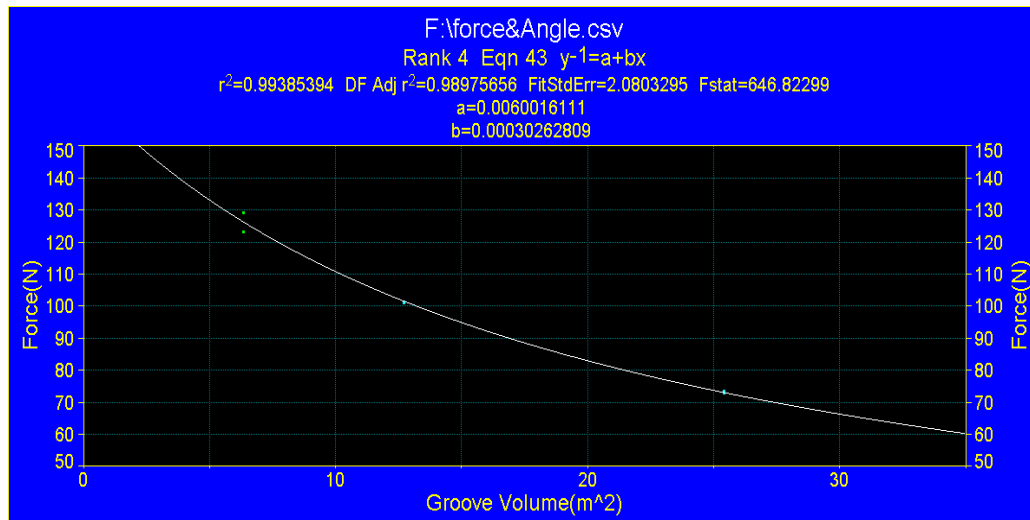
Figure 78: Variation of magnitude of force with cross sectional area
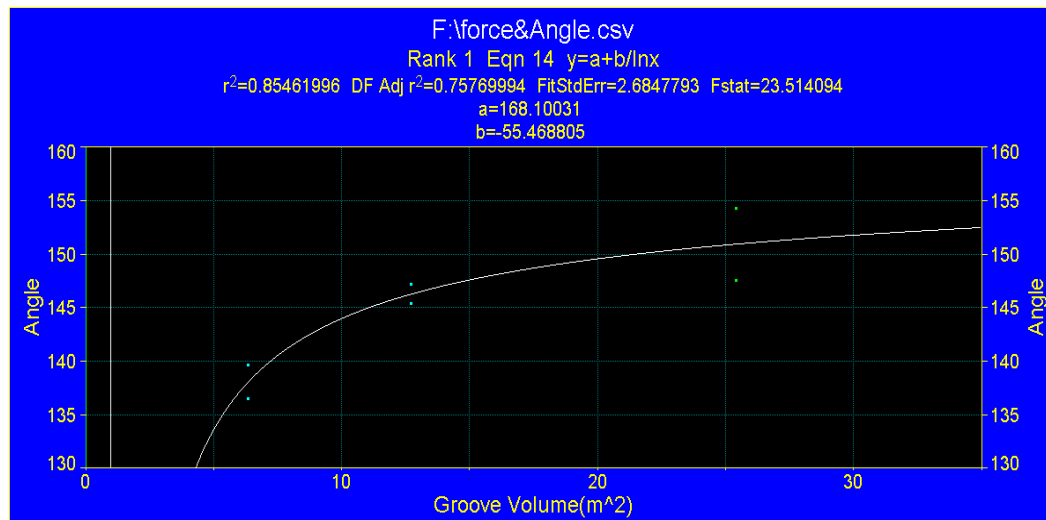
Figure 79: Variation of line of action with cross sectional area

Figures 78 and 79 show curve fit for variation of magnitude of force and line of action with cross sectional area. Magnitude of force fits a linear curve while line of action fits a logarithmic curve.

Table 4: Comparison of forces generated for different configurations of SFD

Frequency(HZ)	Groove Depth(mm)	Groove Length(inch)/F_x	Cross sectional Area(mm^2)/F_y	Resultant
50				
pressure forces		-56.7	172.77	
Viscous forces		0.22	-0.22	
Total Force		-56.48	172.55	**181.56**
Angle				**108.1794**
100				
pressure forces		-75.6	539.01	
Viscous forces		0.69	-0.94	
Total Force		-74.91	538.07	**543.26**
Angle				**97.97543**
100	0.5	0.5	6.35	
pressure forces		-162.19	426.3	
Viscous forces		0.5	-0.8	
Total Force		-161.69	425.5	**455.19**
Angle				**110.863**

The force produce by two dimensional simulations for SFD is 356.41N which is double the value of that produced by three dimensional simulations. Tables 3 & 4 confirm the predicted results that equal volumes have equal effect on force generated; grooves of the same volume generate almost equal magnitude of forces irrespective of groove dimensions. It can also be seen that the addition of the central groove reduces the magnitude of forces generated. At higher speed, the magnitude of force generated is higher causing rigidity to some extent. This can be alleviated by adding a central groove on the squeeze film land.

7. CONCLUSION

The feasibility of applying steady state solver (MRF) in Fluent 12.1 to solve for pressure fields inside SFD was studied. Steady state solver in stationary (absolute) reference frame was used to generate whirling motion of the rotor. The results from CFD simulations were compared against experimental results obtained for the same case by Delgado, A., 2008. The pressures predicted by CFD were slightly higher than experimental results but the trend of the pressure curve was followed. This shift in the pressure values can be attributed to non inclusion of air entrapment effects present in experimental study in CFD simulations. This shift can also be overcome by increasing the percentage of air dissolved in lubricant. When the whirling speed of the rotor was increased the maximum pressure generated in the film land was higher and the spread of minimum pressure was wider. Also at higher speeds the minimum pressure generated was low and cavitation due to these low pressures cause sudden jump of pressure curve in low pressure region. The cavitation occurring in the squeeze film land at higher speeds was due to sudden collapse of gas bubble in low pressure region. Central grooves of different dimensions were used to study the effect of central groove on dynamic pressure profiles of squeeze film dampers. The dimensions of central groove that were simulated in this study are given in Table 5.

Table 5: Dimensions of central groove on SFD

Depth(mm)	Length(inch)	Volume(mm^3)
1	0.5	12.7
2	0.25	12.7
0.5	0.5	6.35
1	0.25	6.35
2	0.5	25.4
4	0.25	25.4

When central groove in the simulated range was added to squeeze film land, the pressures generated were reduced to half the values of that generated when run without any central groove on it. It was also observed that the amount of reduction in pressure values depend on the volume of the groove but not the length and the depth of the groove. Addition of central groove reduces the rigidity developed in the film land when run at higher speeds.

8. FUTURE WORK

Since steady state solution was achieved using Moving Reference Frame:

1. This model can be used to address the effects of higher rotor speeds.

2. In the present study 3% of air was dissolved in lubricant. It would be of interest to know the effects of using different percentages of air dissolved in lubricant.

3. To improve the accuracy of prediction and to accommodate for different types of cavitations other than gaseous cavitation addressed in this study, different models of cavitation other than Singhal cavitation model can be used and tested.

4.   In present study end sealing effects were not included. The accuracy of prediction would improve if end sealing effects are included.

5. It would be of interest to know on how non circular orbits would affect dynamic pressure profiles of squeeze film dampers.

6. In the present study a minimum depth of 0.5 mm is used for central groove. For future work smaller depths than 0.5mm should be studied to see if they have more prominent effect on dynamic pressure profiles of SFD.

7. It is seen that for central groove with depth of 4mm, dimensions of central groove did not have any effect on pressures generated. For future work it can be verified whether this is valid for all grooves with depths greater than 4mm.

REFERENCES

Chen, P., and Hahn, E., J, 1998, "Use of Computational Fluid Dynamics in Hydrodynamic Lubrication," *Proceedings of the Institute of Mechanical Engineers*, 212(Part J).

Delgado, A., 2005, "Identification of Force Coefficients in a Squeeze Film Damper with a Mechanical Seal," M.S, thesis, Texas A&M University, College Station,TX.

Delgado, A., 2008, "A Linear Fluid Inertia Model for Improved Prediction of Force Coefficients in Grooved Squeeze Film Dampers and Grooved Oil Seal Rings," Ph.D, dissertation, Texas A&M University, College Station, TX

El-Shafei, A., 1993, "Experimental and Analytical Investigation of Hybrid Squeeze Film Dampers," *Journal of Engineering for Gas Turbines and Power,* Vol. 115, pp. 353-359.

Feder, E., Bansal, P., and Blanco, A., 1978, "Investigation of Squeeze Film Damper Forces Produced By Circular Centered Orbits," *Journal of Engineering for Power*, Vol. 100, No. 1, pp. 15-21.

Feng, N., S, and Hahn, E., J, 1986, "Cavitation Effects on Squeeze Film Damper Performance," *ASLE Transactions*, Vol. 29, No. 3, pp. 353-360.

Fluent 12.1 Documentation, 2010, "*Fluent 12.1 User's Guide,*" Pennsylvania: ANSYS INC.

Gertzos, K. P., Nikolakopoulos, P. G., and Papadopoulos, C. A., 2008, "CFD Analysis of Journal Bearing Hydrodynamic Lubrication by Bingham Lubricant," *Tribiology International*, Vol. 41, pp. 1190-1204.

Guo, Z., Hirano, T., and Kirk, G., 2005, "Application of CFD Analysis for Rotating Machinery- Part I: Hydrodynamics, Hydrostatic Bearings and Squeeze Film Damper," *Journal of Engineering for Gas Turbines and Power,* Vol. 127, pp. 445-451.

Milind, K., 2011, "Numerical Simulation of Flow Field inside a Squeeze Film Damper and the Study of the Effect of Cavitation on the Pressure Distribution., " M.S, thesis, Texas A&M University, College Station, TX.

San Andres, L., 2008, "MEEN 626 Course Notes," Mechanical Department,Texas A&M University, http://rotorlab.tamu.edu/me626/College Station, TX.

Terdsak, N., 2011, "Numerical Investigation of Flow Fields and Forces for 2-D Squeeze Film Dampers," M.S, thesis, Texas A&M University, College Station, TX.

Thomsen, K., and Andersen, H., 1974, "Experimental Investigation of a Simple Squeeze Film Damper," *Journal of Engineering for Industry*, Vol. 96, No. 2, pp. 427-430.

Vance, J., and Kirton, J., 1975, "Experimental Measurement of the Dynamic Force Response of a Squeeze Film Bearing Damper," *Journal of Engineering for Industry*, Vol. 97, No. 4, pp. 1282-1290.

Xing, C., 2009, "Sealing Effect on Performance of Squeeze Film Damper," *Proceedings of 2009 ASME Turbo Expo: Power for Land, Sea and Air GT*.

Zeidan, F., and Vance, J., 1989, "Cavitation Leading to a Two Phase Fluid in a Squeeze Film Damper," *STLE Tribilogy Transactions*, Vol. 32, No. 1, pp. 100-104.

Zeidan, F., and Vance, J., 1990a, "Cavitation and Air Entrainment Effects on the Response of Squeeze Film Supported Rotors," *ASME Journal of Tribilogy*, Vol. 112, pp. 347-353.

Zeidan, F., and Vance, J., 1990b, "Cavitation Regimes in Squeeze Film Dampers and Their Effect on the Pressure Distribution," *Tribology Transactions*, Vol. 33, No. 3, pp. 447-453.

Zeidan, F., San Andres, L., and Vance, J., 1996, "Design and Application of Squeeze Film Dampers in Rotating Machinery," *Proceedings of the Twenty-Fifth Turbomachinery Symposium, Turbomachinery Laboratory,* Texas A&M University, College Station, TX, pp. 169-188.

APPENDIX A

The Mixture Model

For modeling multiphase flows in squeeze film dampers mixture model in Fluent is used. Here oil air mixture in the clearance is treated as homogenous mixture. This model is designed for solving multiphase flows moving at different velocities and has capability of solving full multiphase model with smaller number of variables than full Eulerian multiphase model. In this model continuity, momentum, and energy equations are solved for mixture while volume fraction equation is solved for secondary phases. While solving these equations local equilibrium over short spatial length scales is assumed.

Relative velocity is assigned to each phase when there is slip between the phases and to solve homogeneous multiphase mixtures (all phases move with same velocity) this relative velocity is turned off. Mixture model can be used only for pressure based solver and Singhal Cavitation model is not compatible with Large Scale Eddy Simulation model. Relative formulation of mixture model cannot be used in combination with MRF model.

Continuity Equation

The continuity equation for mixture is given by

$$\frac{\partial}{\partial t}(\rho_m) + \nabla \cdot (\rho_m \vec{v}_m) = 0$$

where mixture mass-average velocity is given by

$$\vec{v}_m = \frac{\sum_{k=1}^{n} \alpha_k \rho_k \vec{v}_k}{\rho_m}$$

and mixture density by

$$\rho_m = \sum_{k=1}^{n} \alpha_k \rho_k$$

α_k is volume fraction of phase k

Momentum Equation

Momentum equation for mixture is obtained by summing individual momentum equations of all the phases and is given by

$$\frac{\partial(\rho_m \vec{v}_m)}{\partial t} + \nabla \cdot (\rho_m \vec{v}_m \vec{v}_m) = -\nabla p + \nabla \cdot [\mu_m (\nabla \vec{v}_m + \vec{v}_m^T)] + \rho_m \vec{g} + \vec{F} + \nabla \cdot (\sum_{k=1}^{n} \alpha_k \rho_k \vec{v}_{dr,k} \vec{v}_{dr,k})$$

where n is number of phases and F is body force and μ_m is given by

$$\mu_m = \sum_{k=1}^{n} \alpha_k \mu_k$$

Drift velocity for secondary phase k is given by

$$\vec{v}_{dr,k} = \vec{v}_k - \vec{v}_m$$

The suffix m is used for representing mixture properties

Energy Equation

The energy equation for mixture is of the form

$$\frac{\partial}{\partial t} \sum_{k=1}^{n} (\alpha_k \rho_k E_k) + \nabla \cdot \sum_{k=1}^{n} (\alpha_k \vec{v}_k (\rho_k E_k + p)) = \nabla \cdot (k_{eff} \nabla T) + S_E$$

where effective thermal conductivity is given as

$$k_{eff} = \sum \alpha_k (k_k + k_t)$$

K_t being turbulent thermal conductivity and S_E is any heat source

$$E_k = h_k - \frac{p}{\rho_k} + \frac{v^2_k}{2}$$

For incompressible phase $E_k = h_k$ with h_k representing sensible enthalpy of phase k

Volume Fraction Equation

The volume fraction of secondary phase p is obtained from continuity equation of secondary phase p and is given as

$$\frac{\partial}{\partial t}(\alpha_p \rho_p) + \nabla \cdot (\alpha_p \rho_p \vec{v}_m) = -\nabla \cdot (\alpha_p \rho_p \vec{v}_{dr,p}) + \sum_{q=1}^{n}(\dot{m}_{qp} - \dot{m}_{pq})$$

Suffix p is used for representing secondary phase properties.

APPENDIX B

The Standard k- ε model

Turbulence model is used model the turbulence viscosity term or Reynolds shear stress term in modified Navier stokes equation or Reynolds Averaged Navier Stokes equation (RANS). First model for modeling Reynolds shear stress term is given Prandtl which is known as Prandtl mixing length theory. Later many other models for modeling Reynolds shear stress term are developed, of them many researchers have established that for small clearances k- ε model proved to be more useful and provide accurate results for wide range of turbulent flows.

The continuity and momentum equations solved in RANS equation are

$$\frac{\partial \rho}{\partial t} + \frac{\partial}{\partial x_i}(\rho \bar{u}_i) = 0$$

$$\frac{\partial}{\partial t}(\rho \bar{u}_i) + \frac{\partial}{\partial x_j}(\bar{u}_i \bar{u}_j) = -\frac{\partial \bar{p}}{\partial x_i} + \frac{\partial}{\partial x_j}\left[\mu \left(\mu \frac{\partial u_i}{\partial x_j} + \frac{\partial u_j}{\partial x_i} - \frac{2}{3}\delta_{ij}\frac{\partial u_l}{\partial x_l} \right) \right] + \frac{\partial}{\partial x_j}(-\rho \overline{u_i' u_j'})$$

In k- ε model the Reynolds shear stress term $\rho \overline{u_i' u_j'}$ is related to average or mean velocity gradients by the following relation

$$-\rho \overline{u_i' u_j'} = \mu_t \left(\frac{\partial u_i}{\partial x_j} + \frac{\partial u_j}{\partial x_i} \right) - \frac{2}{3}\left(\rho k + \mu_t \frac{\partial u_k}{\partial x_k} \right)\delta_{ij}$$

where μ_t is turbulence viscosity.

The k- ε model was first proposed by Launder and Spalding; it is a semi empirical model and is based on model transport equations for the turbulence kinetic energy (k) and its dissipation rate (ε). The transport equation for k is obtained from the

exact equation, while the transport equation for ε is obtained from physical reasoning.

This model neglects molecular viscosity and is valid for only fully turbulent flows.

For all k- ε models any of the available near wall treatments should be used. They are

1) Standard Wall Functions

2) Non-Equilibrium Wall Functions

3) Enhanced Wall Treatment

4) User-Defined Wall Functions.

For modeling squeeze film dampers using steady state solver standard wall function is used where y plus has to be in the range of 30-300.

The k- ε model is a 2 equation model; turbulence kinetic energy (k) and its dissipation rate (ε) are obtained from following transport equations.

$$\frac{\partial}{\partial t}(\rho k) + \frac{\partial}{\partial x_i}(\rho k u_i) = \frac{\partial}{\partial x_j}\left[\left(\mu + \frac{\mu_t}{\sigma_k}\right)\frac{\partial k}{\partial x_j}\right] + G_k + G_b - \rho\varepsilon - Y_M + S_k$$

$$\frac{\partial}{\partial t}(\rho\varepsilon) + \frac{\partial}{\partial x_i}(\rho\varepsilon u_i) = \frac{\partial}{\partial x_j}\left[\left(\mu + \frac{\mu_t}{\sigma_\varepsilon}\right)\frac{\partial\varepsilon}{\partial x_j}\right] + C_{1\varepsilon}\frac{\varepsilon}{k}(G_k + C_{3\varepsilon}G_b) - C_{2\varepsilon}\rho\frac{\varepsilon^2}{k} + S_\varepsilon$$

G_k represents the production of turbulence kinetic energy due to mean velocity gradients which is given by equation

$$G_k = -\ \rho\overline{u_i'u_j'}\ \frac{\partial uj}{\partial xi} \quad \text{Or } G_k = \mu_t S^2$$

where S and S_{ij} are,

$$S = \sqrt{2S_{ij}S_{ij}}$$

$$S_{ij} = \frac{1}{2}\left(\frac{\partial u_i}{\partial x_j} + \frac{\partial u_j}{\partial x_i} \right)$$

And G_b represents the production of turbulence kinetic energy due to buoyancy which is given by equation

$$G_b = \beta \frac{\mu_t}{\text{Pr}_t} \frac{\partial T}{\partial x_i}$$

Y_M represents the contribution of the fluctuating dilatation in compressible turbulence to the overall dissipation rate

$$Y_M = \frac{2\rho\varepsilon k}{\gamma RT}$$

$C_{1\epsilon}$, $C_{2\epsilon}$, and $C_{3\epsilon}$ are constants. σ_k and σ_ϵ are the turbulent Prandtl numbers for k and ϵ, respectively. S_k and S_ϵ are user-defined source terms. These are determined from experiments and are given by

$C_{1\epsilon} = 1.44$, $C_{2\epsilon} = 1.92$, $\sigma_k = 1$ and $\sigma_\epsilon = 1.3$

From these equations k and ε are solved for and using these values μ_t the turbulence viscosity term is found from equation

$$\mu_t = \rho c_\mu \frac{k^2}{\epsilon}$$

$C_\mu = 0.09$

APPENDIX C

Moving Reference Frame

Moving Reference Frame is a technique used to model and transform an unsteady state problem in stationary reference frame to a steady state problem in moving reference frame. In moving reference frame model, the equations of motion include additional acceleration terms which occur due to the transformation from the stationary to the moving reference frame. For simple geometries Single Reference Frame model can be used while for complex geometries the model has to be split into multiple cell zones. The way these multiple cell zones are treated leads to two different models Multiple Reference Frame and Mixing Plane approach.

For describing equations governing rotating reference frame consider a coordinate system steadily rotating with angular velocity relative to a stationary reference frame, the origin of the rotating system is given by a position vector. Let $\vec{a}$ be the unit direction vector of axis of rotation. Any arbitrary point in CFD domain is represented by vector r from origin of rotating reference frame.
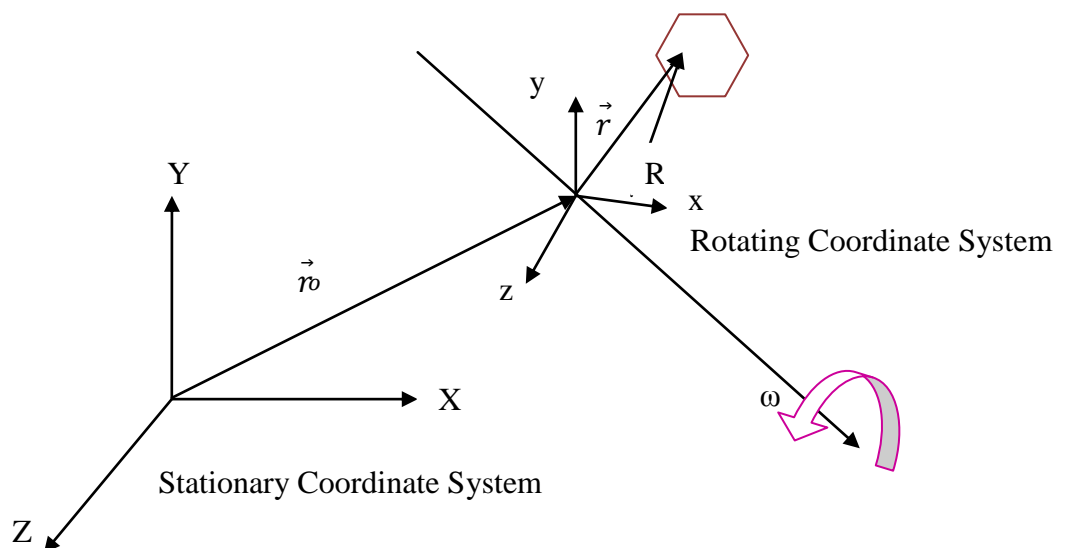
$$\vec{\omega} = \omega \hat{a}$$

The fluid velocities are transformed from stationary reference frame to rotating reference frame using the following relations

$$\vec{v}_r = \vec{v} - \vec{u}_r$$

$$\vec{u}_r = \vec{\omega} \times \vec{r}$$

Equations of motion rotating reference frame have additional acceleration terms and can be solved in two different ways

1) Relative Velocity Formulation where momentum equations are expressed using relative velocities as dependent variables

2) Absolute Velocity Formulation where momentum equations are expressed using absolute velocities as dependent variables

For modeling Squeeze Film Dampers using steady state solver absolute velocity formulation is used. In this formulation coriolis and centripetal acceleration terms are collapsed into a single term. For pressure based solvers both relative velocity and absolute velocity formulations can be used while for density based solvers only absolute velocity formulations can be used. The governing equations of fluid flow with absolute velocity formulation are as follows

Conservation of Mass:

$$\frac{\partial \rho}{\partial t} + \nabla . \rho \vec{v}_r = 0$$

Conservation of Momentum:

$$\frac{\partial \rho \vec{v}}{\partial t} + \nabla . (\rho \vec{v}_r \vec{v}) + \rho (\vec{\omega} \, X \, \vec{v}) = -\nabla p + \nabla . \bar{\bar{\tau}} + \vec{F}$$

Conservation of Energy:

$$\frac{\partial \rho E}{\partial t} + \nabla . (\rho \vec{v}_r H + p\vec{u}_r) = \nabla . (k\nabla T + \bar{\bar{\tau}} . \vec{v}) + S_h$$

In this formulation the Coriolis acceleration term and centripetal acceleration term collapse into single $(\vec{\omega} \; X \; \vec{v})$ term

VITA

Name:	Praneetha Boppa
Address:	Texas A&M University, Department of Mechanical Engineering, 3123 TAMU, College Station TX 77843
Email Address:	boppa.pranitha@gmail.com
Education:	B.Tech., National Institute of Technology Warangal, 2008 M.S., Mechanical Engineering, Texas A&M University, 2011